106 J. Med. Chem. 2010, 53, 106–118
DOI: 10.1021/jm9013532

Journal of Medicinal Chemistry Article

Antiangiogenic Effect of Dual/Selective $\alpha_5\beta_1/\alpha_v\beta_3$ Integrin Antagonists Designed on Partially Modified Retro-Inverso Cyclotetrapeptide Mimetics

Luca Gentilucci,*,† Giuliana Cardillo,† Santi Spampinato,‡ Alessandra Tolomelli,† Federico Squassabia,§ Rossella De Marco,† Andrea Bedini,‡ Monica Baiula,‡ Laura Belvisi,∥ and Monica Civera∥

†*Department of Chemistry "G. Ciamician", Università degli Studi di Bologna, via Selmi 2, 40126 Bologna, Italy,* ‡*Department of Pharmacology, Università degli Studi di Bologna, via Irnerio 48, 40126 Bologna, Italy,* §*Stepbio srl, Bologna, Via P. Nanni Costa 12/3/e-f, 40133 Bologna, Italy, and* ∥*Department of Organic and Industrial Chemistry and CISI, University of Milano, Via Venezian 21, Milano, Italy*

Received May 20, 2009

Recent evidence highlighted the role of $\alpha_5\beta_1$ integrin in angiogenesis and in regulating $\alpha_v\beta_3$ integrin function. As a consequence, selective $\alpha_5\beta_1$ integrin inhibitors or dual $\alpha_5\beta_1/\alpha_v\beta_3$ integrin inhibitors are considered promising candidates for the development of cancer therapeutic agents. In this paper, we describe the synthesis and pharmacological characterization of a minilibrary of cyclotetrapeptide mimetics containing a PMRI Arg-Gly-Asp sequence. In particular, c[(*R*)-β-Pheψ(NHCO)Aspψ-(NHCO)Gly-Arg] (**3**) displayed a good activity in inhibiting the $\alpha_v\beta_3$ integrin-mediated cell adhesion of fibronectin or vitronectin, as well as the adhesion of fibronectin to the $\alpha_5\beta_1$ integrin. Interestingly, the diastereomeric compound c[(*S*)-β-Pheψ(NHCO)Aspψ(NHCO)Gly-Arg] (**2**) maintained a good efficacy in inhibiting $\alpha_5\beta_1$ integrin while gaining a certain selectivity over $\alpha_v\beta_3$ integrin. These two integrin antagonists significantly inhibited bFGF-induced human endothelial cell tube formation at submicromolar concentrations. Conformational analysis and Molecular Docking calculations suggest that the different $\alpha_5\beta_1$ versus $\alpha_v\beta_3$ selectivity of **2** and **3** can be rationalized on the basis of the alternative display of the aromatic side chain adjacent to Asp.

Introduction

Among the different members of the integrin receptor family, $\alpha_v\beta_3$ integrin is generally considered a privileged target for antiangiogenic therapy.[1−6] At the same time, $\alpha_5\beta_1$ integrin has emerged as a new promising target for the development of cancer therapeutic agents. Besides an important function in the migration of activated lymphocytes during the immune response and the involvement in diabetes and inflammatory diseases like rheumatoid arthritis,[7] the proangiogenic function of the $\alpha_5\beta_1$ receptor has been clearly demonstrated.[8]

Interestingly, the $\alpha_5\beta_1$ integrin has been shown to affect $\alpha_v\beta_3$-mediated endothelial cell migration and angiogenesis via regulation of $\alpha_v\beta_3$ integrin function.[9] A study with $\alpha_v\beta_3$ and $\alpha_5\beta_1$ specific antibodies demonstrated that integrin $\alpha_5\beta_1$ regulates the function of integrin $\alpha_v\beta_3$ on endothelial cells during their migration in vitro or angiogenesis in vivo.[10] Likewise, it has been reported that the combined antagonism of both $\alpha_v\beta_3$ and $\alpha_5\beta_1$, as opposed to $\alpha_v\beta_3$ alone, induces apoptosis of angiogenic endothelial cells cultured on type I collagen.[11]

Another approach to developing integrin inhibitors is to modify extracellular matrix proteins like angiostatin, tamustatin, arresten, and endostatin capable of antagonizing $\alpha_v\beta_3$ and $\alpha_5\beta_1$.[12] A laminin-1-derived peptide that similarly blocks $\alpha_v\beta_3$ and $\alpha_5\beta_1$ has been shown to inhibit growth of melanoma cells in vivo.[13]

The endogenous extracellular matrix ligands vitronectin and fibronectin bind to the $\alpha_v\beta_3$ integrin, and fibronectin binds also to $\alpha_5\beta_1$ integrin by recognition of the acidic and guanidino side chain groups of the same tripeptide motif, the Arg-Gly-Asp (RGD)[a] sequence.[14] Therefore, small RGD-mimetic molecules that are able to interfere with the $\alpha_5\beta_1$ and/or $\alpha_v\beta_3$ integrins are currently considered of interest for the angiostatic therapy of cancer.[15−17] The RGD sequence is the recognition site for various integrin receptors, and the conformation of the sequence in the individual adhesion protein or peptide is critical for the specificity of this recognition.[18,19]

*To whom correspondence should be addressed. E-mail: luca.gentilucci@unibo.it. Phone: +39 0512099462. Fax: +39 0512099456.

[a] Abbreviations: bFGF, basic fibroblast growth factor; RGD, Arg-Gly-Asp; CTP, cyclotetrapeptide; PMRI, partially modified retro-inverso; 2D and 3D, two- and three-dimensional, respectively; Cbz, benzyloxycarbonyl; Fmoc, fluorenylmethyloxycarbonyl; Bz, benzyl; DPPA, diphenylphosphoryl azide; TFA, trifluoroacetic acid; EDCI, *N*-[3-(dimethylamino)propyl]-*N*′-ethylcarbodiimide; HOBt, 1-hydroxybenzotriazole; TEA, triethylamine; DCM, dichloromethane; DMF, *N*,*N*-dimethylformamide; DMA, dimethylamine; THF, tetrahydrofuran; DMSO, dimethyl sulfoxide; K562, human erythroleukemic cells; SK-MEL-24, human malignant melanoma cells; HUVEC, human umbilical vein endothelial cells; BSA, bovine serum albumin; ECM, extracellular matrix; SEM, standard error of the mean; ANOVA, analysis of variance test; MD, molecular dynamics; VT, variable temperature; rmsd, root-mean-square deviation; AMBER, assisted model building with energy refinement; TIP3P, transferrable intermolecular potential three point; MIDAS, metal ion-dependent adhesion site; CPK, Corey, Pauling, and Koltun; DAD, diode array detector; ODS, octadecyl silane; EDTA, ethylenediaminetetraacetic acid; MEM, minimum essential medium; RPMI, Roswell Park Memorial Institute; FBS, fetal bovine serum; PBS, phosphate-buffered saline; PMA, phorbol 12-myristate 13-acetate; PI, propidium iodide; HMBC, heteronuclear multiple-bond coherence; HSQC, heteronuclear single-quantum coherence; rt, room temperature.

 Published on Web 11/30/2009

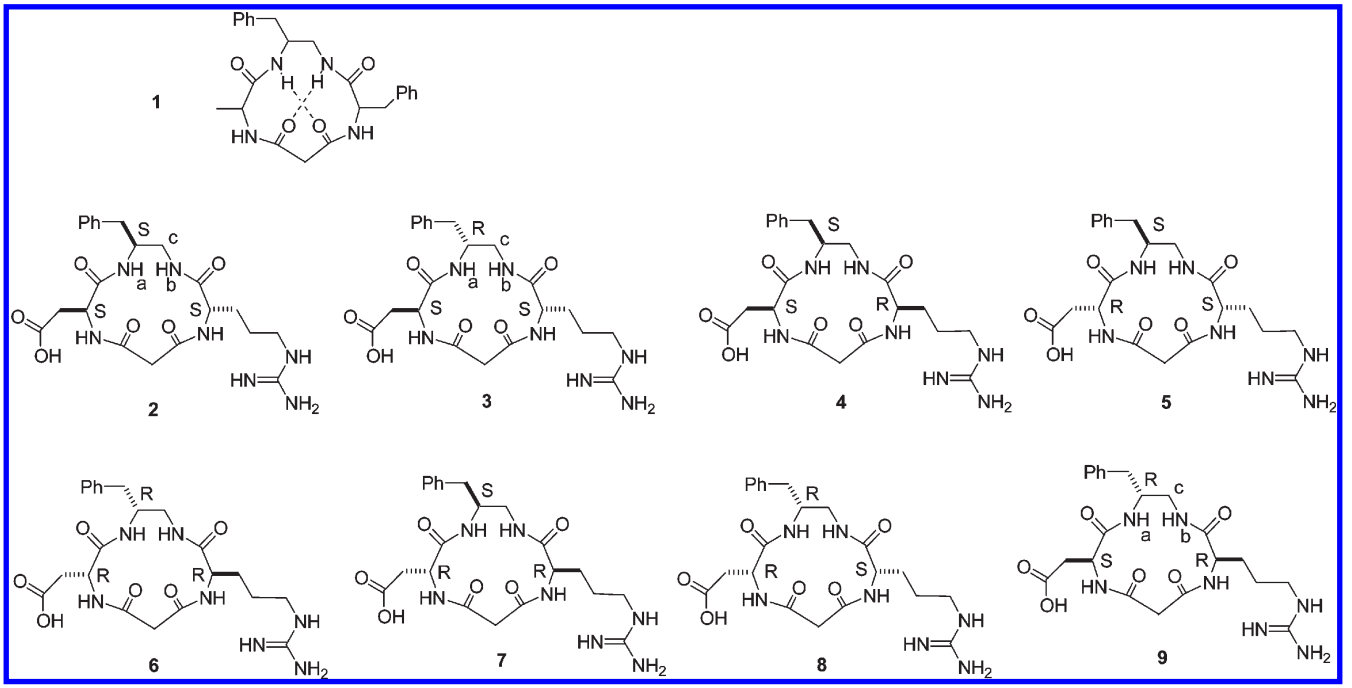

Figure 1. General structure of the PMRI−cyclotetrapeptide models c[(*S*/*R*)-βPheψ(NHCO)(*S*/*R*)-Alaψ(NHCO)Gly-(*S*/*R*)-Phe] **1** and structures of stereoisomeric PMRI RGD mimetics c[(*S*/*R*)-βPheψ(NHCO)(*S*/*R*)-Aspψ(NHCO)Gly-(*S*/*R*)-Arg] **2**−**9**.

With regard to the $\alpha_v\beta_3$ integrin receptor, a large number of peptidic, peptidomimetic,[20,21] and nonpeptidomimetic[22] scaffolds have been successfully employed to provide the desired conformational constraint to maintain the acidic and basic side chains at the appropriate distance and in a conformation suitable for binding. The cyclopentapeptide c[Arg-Gly-Asp-(*R*)-Phe-Val] has represented the first highly active and selective $\alpha_v\beta_3$ integrin antagonist[23−25] and has served as a lead structure for the development by Kessler et al. of the cyclic pentapeptide cilengitide, c[Arg-Gly-Asp-(*R*)-Phe-NMeVal] (EMD121974),[26] currently in clinical trials for antiangiogenic cancer therapy.[27,28] Furthermore, the crystal structure of the extracellular segment of the $\alpha_v\beta_3$ integrin with cilengitide bound to the active site has been disclosed previously,[29] giving the opportunity to design novel integrin antagonists based on the receptor-bound conformation of the RGD tripeptide.[30]

On the other hand, the experimental 3D structure of $\alpha_5\beta_1$ integrin is not available, and few structural details about ligand−receptor interactions have been obtained until now.[31,32] As a consequence, only some potent and selective antagonists of $\alpha_5\beta_1$ or dual $\alpha_5\beta_1/\alpha_v\beta_3$ antagonists have been described.[33−36] Recently, a homology model of the receptor has been published,[37] which has successfully been used to optimize ligand activity and selectivity.[38]

In essence, the criteria for designing integrin antagonists showing selectivity for a certain RGD-binding integrin type over the others seem to reside for the most part in subtle differences in the reciprocal orientation and distance between the Asp and Arg side chains, and in the disposition of an aromatic side chain adjacent to Asp. In particular, the presence of definite secondary structure elements in RGD linear or cyclic peptides has often been correlated to the ligand's specificity.[20,30,31,38] Therefore, the synthesis of novel, conformationally definite RGD-containing scaffolds to mimic important secondary structure elements such as γ- or β-turns is of great interest.

Very recently,[39,40] we designed a new kind of cyclotetrapeptide (CTP) scaffold based on a partially modified retro-inverso (PMRI) variant of CTP containing a β-amino acid, forming 13-membered rings.[41] Retro-inverso and PMRI analogues have been widely utilized to improve the performance of a bioactive parent peptide.[42−46] We envisaged the opportunity to utilize these scaffolds for designing peptidomimetic molecules with a well-defined 3D display of the RGD sequence and aimed to discover selective $\alpha_5\beta_1$ integrin antagonists or dual $\alpha_v\beta_3/\alpha_5\beta_1$ integrin antagonists, whose activity could be synergistically effective in preventing angiogenesis.

Results

Design and Synthesis. Compared to CTPs composed of all α-amino acids, which can be considered the smallest turn-mimetic structure, 13-membered analogues incorporating a β^3- or β^2-amino acid proved to be easier to synthesize and conformationally more defined.[41,47−49] The eight stereoisomeric PMRI−CTP models (**1**) of the general sequence c[(*S*/*R*)-βPheψ-(NHCO)(*S*/*R*)-Alaψ(NHCO)Gly-(*S*/*R*)-Phe] (Figure 1) contain a 1,2-diamine to replace the β-amino acid, and a diacid as a Gly mimetic. Conformational analysis revealed that these 13-membered scaffolds manifest specific 3D geometries in comparison to normal 13-membered CTPs[39] and have a strong tendency to adopt turn structures. This preference can be ascribed to the propensity of the PMRI−CTP structures to stabilize H-bonded conformations involving the diamine amide protons.[50]

On the basis of the structures of the scaffolds **1**, we designed a minilibrary of PMRI RGD-mimetic compounds,[21] aiming to obtain integrin antagonists having the pharmacophoric side chains in well-defined, predictable spatial dispositions. For this purpose, we prepared the stereoisomeric compounds c[(*S*/*R*)-βPheψ(NHCO)(*S*/*R*)-Aspψ(NHCO)Gly-(*S*/*R*)-Arg] **2**−**9** by introducing (*S*)- or (*R*)-Asp and (*S*)- or (*R*)-Arg in place of (*S*)- or (*R*)-Ala and (*S*)- or (*R*)-Phe, respectively (some preliminary results of the

Scheme 1. Synthesis of **2**[a]

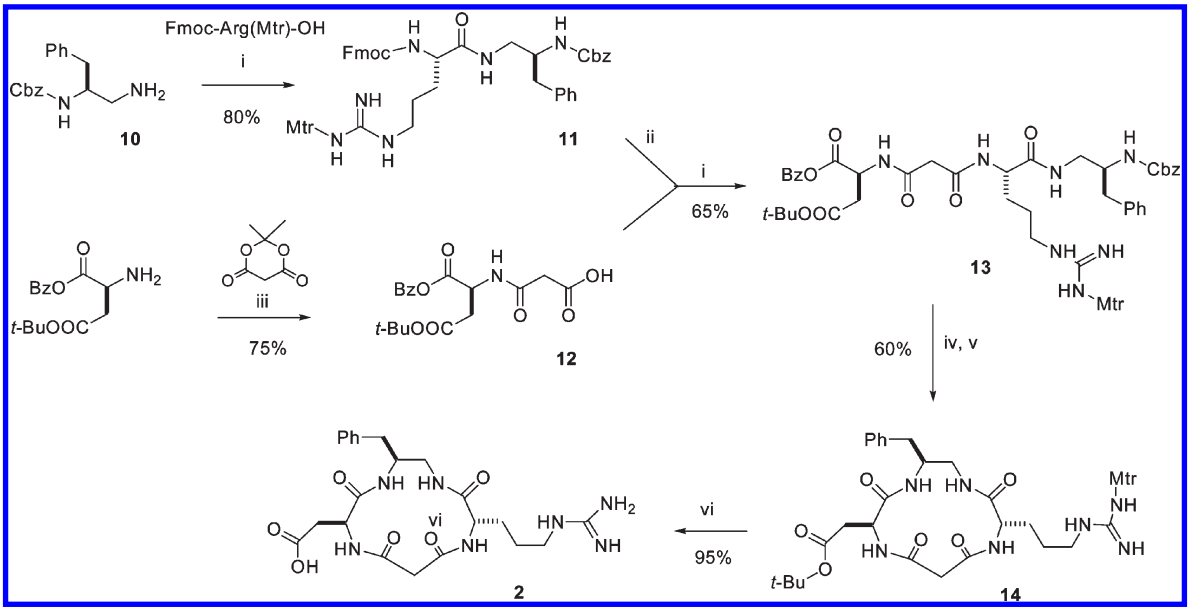

[a] (i) EDCI/HOBt/TEA, DCM/DMF; (ii) DMA/THF; (iii) CH_3CN, 70 °C; (iv) H_2, Pd/C, EtOH; (v) DPPA/$NaHCO_3$, DMF; (vi) 94:2:1:2:1 TFA/PhOH/PhSH/H_2O/Et_2S.

Table 1. Analytical Characterization of **2**−**9** and Inhibition of $\alpha_v\beta_3$ and $\alpha_5\beta_1$ Integrin-Mediated Cell Adhesion to Fibronectin (FN) and Vitronectin (VN) in the Presence of **2**−**9**, or Reference Cyclic Peptide c[Arg-Gly-Asp-(*R*)-Phe-Val] and Negative Control Peptide c[Arg-Ala-Asp-(*R*)-Phe-Val], c[RGDfV] and c[RADfV], Respectively, in Brief

compd	purity (%)	MS [M + 1][a]	$\alpha_v\beta_3$ vs FN (SK-MEL-24) IC_{50} (μM)[b]	$\alpha_v\beta_3$ vs VN (HUVEC) IC_{50} (μM)[b]	$\alpha_5\beta_1$ vs FN (K562) IC_{50} (μM)[b]
2	97	490.2	11 ± 6	25.2 ± 5.2	0.52 ± 0.04
3	96	490.3	0.18 ± 0.05	0.24 ± 0.08	0.024 ± 0.003
4	95	490.3	2.3 ± 0.3	1.5 ± 0.4	4.7 ± 0.4
5	95	490.4	> 100	> 100	> 100
6	95	490.2	> 100	> 100	> 100
7	95	490.1	> 100	> 100	> 100
8	96	490.2	2.1 ± 0.3	0.92 ± 0.09	1.3 ± 0.1
9	96	490.3	> 100	> 100	> 100
c[RGDfV][c]	−	−	7.1 ± 2.7	9.6 ± 2.9	34.7 ± 8.4
c[RADfV][c]	−	−	> 100	> 100	> 100

[a] Calculated [M + 1] of 490.2. [b] Values are means ± the standard error of three experiments conducted in quadruplicate. [c] Purchased from Bachem.

$\alpha_v\beta_3$ integrin-mediated cell adhesion inhibition in the presence of **2**−**4** and **8**, at a single concentration, have been reported in a previous paper[50]).

The cyclic PMRI RGD mimetics were easily obtained from the corresponding linear precursors. As a prototypic example, the synthesis of **2**, the first member of the mini-library, is shown in Scheme 1, the syntheses of the other stereoisomers (**3**−**9**) being the same.

The retrosynthetic analysis of the protected linear precursor **13** was thought to proceed by in-solution coupling of fragments **11** and **12**. Reduction of Cbz-Phe-NH_2[51] with BH_3[52] gave chiral Cbz-1,2-diamine **10** in excellent yield. The coupling of **10** under standard conditions with Fmoc-Arg-(Mtr)-OH afforded dipeptide **11**, whose deprotection was performed by treatment with 2 M DMA in THF.

The second fragment was straightforwardly prepared from Meldrum's acid and H-Asp(O*t*-Bu)-OBz, giving dipeptide acid **12**, not needing further deprotection steps. The standard coupling of dipeptides **11** and **12** gave fully protected linear tetrapeptide **13**. The removal of the Cbz and benzyl ester protecting groups at the N- and C-termini, respectively, by hydrogenolysis, followed by cyclization with DPPA, gave cyclopeptide **14** in good yield and purity after preparative RP-HPLC. The final deprotection of Asp and Arg side chains was performed with TFA in the presence of a mixture of scavengers. PMRI−CTP **2** was isolated by preparative RP-HPLC.

Accordingly, we prepared the remaining PMRI RGD analogues **3**−**9**; purities and mass characterizations are reported in Table 1.

Inhibition of Cell Adhesion. The ability of compounds **2**−**9** to inhibit the adhesion of K562 (human erythroleukemic cells, expressing $\alpha_5\beta_1$ integrin) or SK-MEL-24 (human malignant melanoma cells, expressing $\alpha_v\beta_3$ integrin) to immobilized fibronectin and the adhesion of HUVEC (human umbilical vein endothelial cells, expressing $\alpha_v\beta_3$ integrin) to immobilized vitronectin was evaluated. These cell models are widely used to investigate potential antagonists of $\alpha_v\beta_3$ integrin (HUVEC and SK-MEL-24)[53,54]or of $\alpha_5\beta_1$ integrin (K562).[55] In these experiments, the cells were seeded onto plates coated with different substrata and allowed to adhere before quantitation of the number of adherent cells. Under these conditions, no significant cell adhesion was observed for BSA-coated plates (negative control) or nonspecific

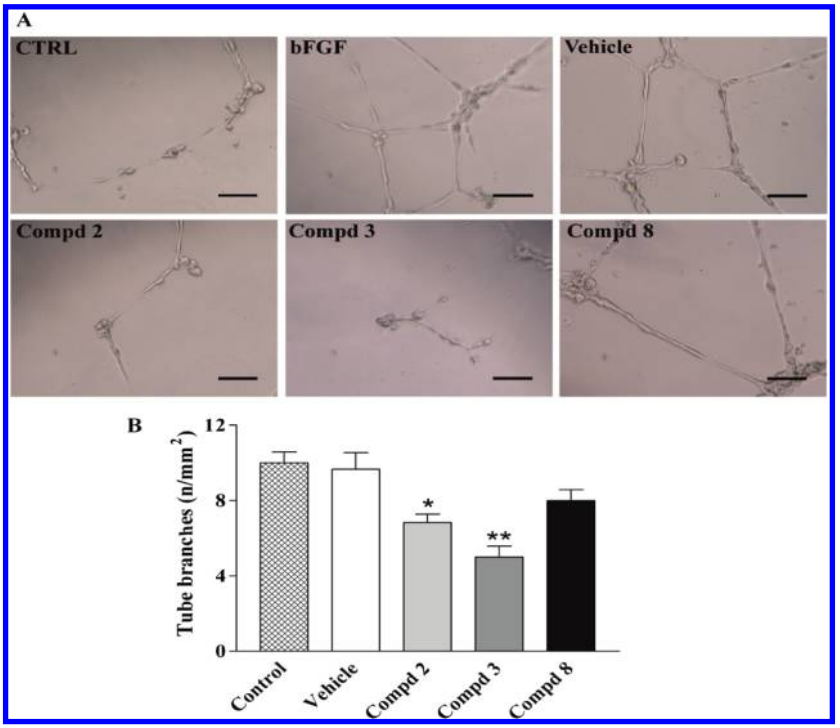

Figure 2. $\alpha_v\beta_3/\alpha_5\beta_1$ integrin antagonists inhibit bFGF-induced tube formation in HUVEC on Matrigel. (A) Representative pictures of capillary-like structures (the black bar in the pictures corresponds to 100 μm): (CTRL) HUVEC plated on Matrigel in the absence of bFGF, (bFGF) HUVEC plated on Matrigel in the presence of bFGF (30 ng/mL) for 16 h, (Vehicle) HUVEC treated with vehicle alone (containing up to 1% DMSO dissolved in cell culture medium), (Compd2) HUVEC treated with compound **2** (1 μM), (Compd3) HUVEC treated with compound **3** (1 μM), and (Compd8) HUVEC treated with compound **8** (10 μM). (B) The ability to form capillary-like sproutings on Matrigel was significantly diminished when HUVEC were treated with compounds **2** and **3**. Data are presented as means ± SEM of the number of tubes per square millimeter. These experiments were conducted in quadruplicate and repeated three times. One asterisk indicates $P < 0.01$, and two asterisks indicate $P < 0.05$ vs control (Newman−Keuls test after ANOVA).

substrate-coated plates (i.e., collagen I for SK-MEL-24 and HUVEC expressing $\alpha_v\beta_3$ integrin and vitronectin for K562 expressing $\alpha_5\beta_1$ integrin) (data not shown). Results are summarized in Table 1. The compound c[Arg-Gly-Asp-(*R*)-Phe-Val] was included as reference cyclic peptide, being a potent inhibitor of cell adhesion,[23,56,57] and the peptide c[Arg-Ala-Asp-(*R*)-Phe-Val] was used as a negative control.[58]

Compound **3**, c[(*R*)-βPheψ(NHCO)Aspψ(NHCO)Gly-Arg], containing (*S*)-Arg and (*S*)-Asp, exhibited the highest potency as an inhibitor of cell adhesion mediated by $\alpha_v\beta_3$ and $\alpha_5\beta_1$ integrins. The IC_{50} value versus $\alpha_5\beta_1$ integrin-mediated cell adhesion was 10 times lower than that versus $\alpha_v\beta_3$ integrin (Table 1). The diastereoisomer **2**, c[(*S*)-βPheψ-(NHCO)Aspψ(NHCO)Gly-Arg], which differs from **3** exclusively for the stereochemistry of the diamine moiety, maintained a notable efficacy as $\alpha_5\beta_1$ integrin inhibitor and gained selectivity versus $\alpha_v\beta_3$ integrin. Indeed, although **2** exhibited an IC_{50} of 0.52 μM as an $\alpha_5\beta_1$ integrin antagonist, the activity toward $\alpha_v\beta_3$ integrin dropped to an IC_{50} value of 11 μM against fibronectin and of 25.2 μM against vitronectin. PMRI RGD mimetic **4** containing (*S*)-Asp and (*R*)-Arg, and mimetic **8** containing (*R*)-Asp and (*S*)-Arg, gave comparatively inferior results with respect to **2** and **3**. Both compounds exhibited modest IC_{50} values, in the micromolar range (Table 1). The rest of the compounds poorly affected adhesion of cells to immobilized fibronectin or vitronectin, with an IC_{50} of > 100 μM.

Compounds **2**−**4** and **8** possess IC_{50} values comparable to those of $\alpha_v\beta_3$ integrin inhibitors in the two cell models expressing this integrin toward the two ligands fibronectin (employed in SK-MEL-24) and vitronectin (employed in HUVEC).[59,60]

In agreement with previous studies,[23,56,57,61] c[Arg-Gly-Asp-(*R*)-Phe-Val] displayed a micromolar inhibitory activity on the cell adhesive capacity driven by $\alpha_v\beta_3$ and $\alpha_5\beta_1$ integrin, whereas the cyclic peptide c[Arg-Ala-Asp-(*R*)-Phe-Val] had IC_{50} values of > 100 μM. Interestingly, compound **3** was more potent than reference compound c[Arg-Gly-Asp-(*R*)-Phe-Val] as it inhibited cell adhesion mediated by $\alpha_v\beta_3$ and $\alpha_5\beta_1$ integrin possessing IC_{50} values 40- and 1445-fold less, respectively.

Effect of Integrin Antagonists on in Vitro Angiogenesis Elicited by Basic Fibroblast Growth Factor (bFGF). The formation of capillary-like tube structures by HUVEC in the extracellular matrix (ECM) is the pivotal step in angiogenesis and is also involved in cell migration and invasion.[62−64] To evaluate any potential antiangiogenic activity of these novel $\alpha_v\beta_3/\alpha_5\beta_1$ integrin antagonists, in vitro angiogenesis assays were conducted by evaluating bFGF-induced angiogenesis of HUVEC cultured in a 3D gel consisting of Matrigel. As shown in Figure 2, when HUVEC were plated on wells coated with Matrigel without the addition of the growth factor, they showed only a few spontaneous tube formations (taken as an index of neo-angiogenesis), and most of them were still in a highly proliferating state with a cobblestone shape. On the other hand, when HUVEC were plated on Matrigel with addition of bFGF (30 ng/mL), cells formed a capillary-like network within 16 h (Figure 2). In the presence of compounds **2** and **3** (1 μM), the extent of tube formation induced by bFGF was significantly reduced (Figure 2) in comparison to that in cells treated with the vehicle alone (containing up to 1%

Table 2. $\Delta\delta/\Delta t$ Values (ppb/K) of Amide Protons for **2** and **3**, Determined by VT ^{1}H NMR Analysis in an 8:2 DMSO-d_6/H_2O Mixture at 400 MHz over the Range of 298−348 K [NHa and NHb (see Figures 1 and 3−6)]

compd	AspNH	ArgNH	NHa	NHb
2	−6.1	−5.8	1.4	−0.6
3	−6.3	−5.0	−4.0	−1.0

DMSO dissolved in cell culture medium). Interestingly, **3** exhibited the greatest inhibitory effect in blocking bFGF-induced angiogenesis. The number of tube branches per square millimeter was reduced from 10 ± 3 (bFGF-treated HUVEC) to 5.1 ± 0.7 (**3**-treated HUVEC), and 6.8 ± 0.9 (**2**-treated HUVEC). The minimal concentration of these compounds yielding a complete inhibition of endothelial morphogenesis on Matrigel was 1 μM; lower concentrations (100 and 500 nM) were less effective or (10 nM) ineffective (data not shown), whereas compound **8** (10 μM) did not cause any significant reduction in the level of angiogenesis (Figure 2). Similarly, compounds **4**−**7** and **9**, added to the cells to a final concentration of up to 10 μM, were not effective as angiogenesis inhibitors (see the Supporting Information).

$\alpha_5\beta_1/\alpha_v\beta_3$ Integrin Antagonists Do Not Affect Endothelial Cell Viability. To determine whether $\alpha_5\beta_1$ and $\alpha_v\beta_3$ integrin antagonists could alter endothelial cell viability, morphology and flow cytometric analysis were evaluated in HUVEC after treatment for 16 h with 1 and 10 μM RGD cyclopeptides. These data indicate that neither significant changes in the morphology (data not shown) nor significant increases in the level of apoptosis or necrosis (Supporting Information) were observed in endothelial cells, suggesting that these compounds do not display any relevant cytotoxicity in HUVEC.

Conformational Analysis of 2 and 3 in Solution. The biological activities of some of the compounds vary radically (Table 1), although the sequence of the peptides is identical. This observation confirms the anticipation that RGD-mimetic compounds based on the PMRI CTPs behave as topologically distinct structures. It is accepted that the conformation of a cyclic peptide is controlled by the stereochemistry array of the residues, while the precise nature of the residues has a minor impact.[21,65,66] In this section, we discuss the in-solution structural features of **2** and **3**, aiming to deduce useful clues about the biologically active structures of this class of pseudopeptides, while the conformations of the less active or inactive compounds **4** and **5** are discussed in the Supporting Information. The conformations of **6**−**9**, the mirror images of **2**−**5**, respectively, were not re-examined.

The conformational analyses were performed by NMR spectroscopy and molecular dynamics (MD) simulations. The NMR analyses of cyclopeptides **2** and **3** were conducted using standard techniques in the 8:2 DMSO-d_6/H_2O biomimetic medium.[67] We could not perform experiments in water, since the peptides were very poorly soluble. The ^{1}H NMR analyses of **2** and **3** revealed a single set of resonances, suggesting conformational homogeneity or a fast equilibrium.[21,65]

VT ^{1}H NMR experiments were utilized to deduce the presence of H-bonds (Table 2). The analyses indicated that in the two cyclopeptides, AspNH and ArgNH do not seem to be involved in intramolecular H-bonds. On the other hand, for both compounds, diamineNHb [NHa, NHb, and Hc (see Figures 1 and 3−6)] very likely participates in a strong H-bond ($|\Delta\delta/\Delta t| \leq 1$ ppb/K).[65,68] With regard to diamineNHa, while in **2** the low $\Delta\delta/\Delta t$ value is suggestive of the involvement in H-bonds ($\Delta\delta/\Delta t$ = 1.4 ppb/K), the comparatively higher $|\Delta\delta/\Delta t|$ value observed in **3** accounts for solvent-exposed protons ($\Delta\delta/\Delta t = -4.0$ ppb/K).

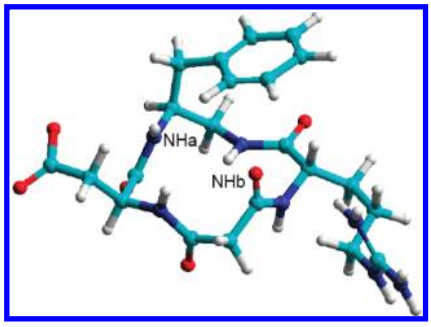

Figure 3. Representative structure of **2** consistent with ROESY analysis.

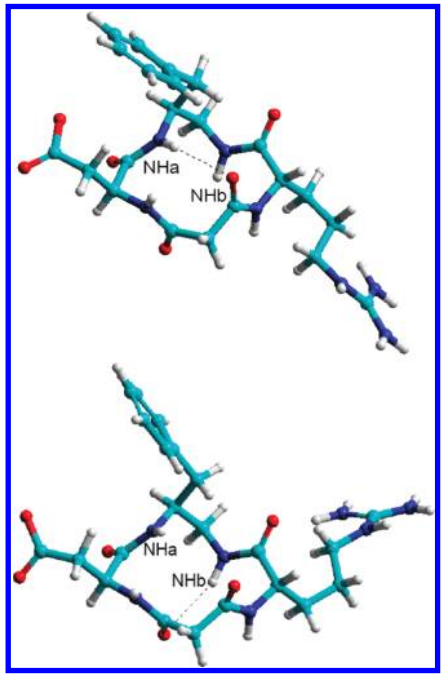

Figure 4. Representative, minimized structures of **2a** (top) and **2b** (bottom) calculated by unrestrained MD in a 30 Å × 30 Å × 30 Å box of standard TIP3P water molecules, characterized by explicit H-bonds and secondary structural elements.

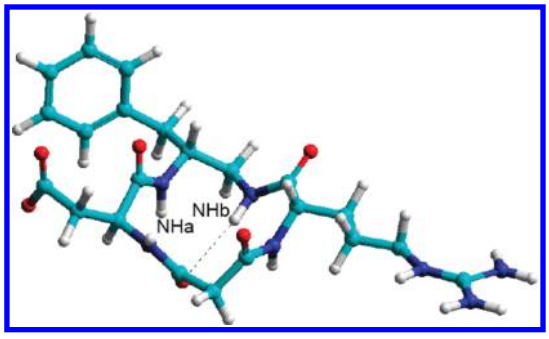

Figure 5. Representative structure of **3a** consistent with ROESY analysis.

2D ROESY data were utilized to investigate the spatial disposition of molecular backbones (Tables 3 and 4). For the absence of $H\alpha_i-H\alpha_{i+1}$ cross-peaks, indicative of a cis peptide bond conformation, all of the ω bonds were set to 180°.

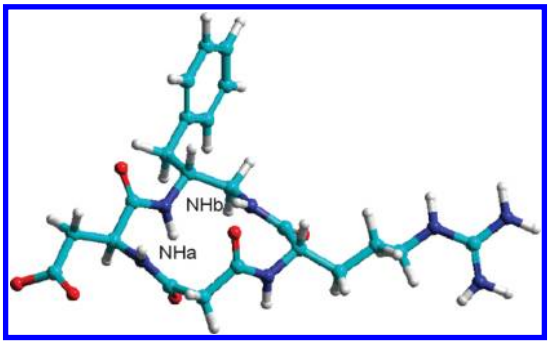

Figure 6. Representative, minimized structure of **3b** calculated by unrestrained MD in a 30 Å × 30 Å × 30 Å box of standard TIP3P water molecules, characterized by secondary structural elements.

Table 3. Nonobvious ROESY Cross-Peaks Observed for **2**[a]

cross-peak	intensity	cross-peak	intensity
AspNH−NHa	s	AspNH−AspHα	m
AspNH−$COCH_2CO_u$	vs	AspNH−AspHβ_d	m
ArgNH−NHb	s	ArgNH−ArgHα	m
ArgNH−$COCH_2CO_d$	vs	ArH−NHb	m
ArH−NHa	s	ArH−diamHα	m
ArH−diamHβ	vs	NHb−NHa	m
NHb−ArgHα	m	NHb−Hc	m
NHa−AspHα	m	NHa−diamHα	s
NHa−diamHβ	s	AspHα−AspHβ_d	m
AspHα−AspHβ_u	w	ArgHα−ArgHβ	s
ArgHα−ArgHγ	w	ArgHα−ArgHδ	m
diamHα−Hc	s	diamHα−diamHβ	s
ArgHδ−ArgHβ	w	ArgHδ−ArgHγ	s
ArgHβ−ArgHγ	s		

[a] Stereochemistry has been omitted. For Ha, Hb, and Hc, see Figure 1. Abbreviations: u, upfield; d, downfield; vs, very strong; s, strong; m, medium; w, weak.

Table 4. Nonobvious ROESY Cross-Peaks Observed for **3**[a]

cross-peak	intensity	cross-peak	intensity
AspNH−NHa	w	AspNH−AspHα	m
AspNH−$COCH_2CO_u$	vs	ArgNH−ArgHα	m
ArgNH−NHb	m	ArH−diamHα	s
ArgNH−$COCH_2CO_d$	vs	ArH−diamHβ_u	vs
ArH−NHa	m	NHb−NHa	m
ArH−diamHβ_d	s	NHb−diamHα	m
NHb−ArgHα	s	NHb−Hc_d	m
NHb−Hc_u	vs	NHa−diamHα	m
NHa−AspHα	vs	AspHα−AspHβ_u	vs
NHa−diamHβ	m	ArgHα−ArgHβ_u	m
ArgHα−ArgHγ	s	ArgHα−ArgHδ	m
diamHα−Hc_d	m	diamHα−Hc_u	s
diamHα−diamHβ_d	s	diamHα−diamHβ_u	s
ArgHβ−ArgHγ	vs	ArgHδ−ArgHγ	s

[a] Stereochemistry has been omitted. For Ha, Hb, and Hc, see Figure 1. Abbreviations: u, upfield; d, downfield; vs, very strong; s, strong; m, medium; w, weak.

Conformations consistent with the spectroscopic analysis were obtained by restrained MD in a box of explicit, equilibrated water molecules,[69] using the distances deduced from ROESY as constraints and minimized with the AMBER[70] force field. A set of 50 random structures generated by means of a unrestrained high-temperature MD simulation was subjected to restrained MD with a scaled force field, followed by a high-temperature simulation with full restraints, after which the system was gradually cooled. These structures were clustered by the rmsd analysis of the backbone atoms. For both peptides, one major cluster comprising more than 90% of the structures was obtained; the lowest-energy structures of the major clusters are shown in Figures 3 and 5.

The ROESY-derived structure of **2** (Figure 3) does not show explicit H-bonds, which were predicted on the basis of the VT NMR analysis. Apparently, the conformations determined by ROESY analyses represent the average on the NMR time scale of different geometries in equilibrium.[21,65]

To estimate the residual flexibility of the cyclopeptide, the dynamic behavior of the structure derived from ROESY was analyzed by unrestrained MD for 10 ns in a box of explicit water. During the simulation, the main structural features described on the basis of ROESY were maintained. In addition, the examination of the trajectories revealed the occurrence of explicit H-bonds in agreement with VT NMR analysis.

Indeed, the trajectories of **2** clearly revealed the occurrence of two slightly different backbone structures. One is characterized by a type I β-turn centered on Arg-diamine and stabilized by a H-bond between malonylCO and diamine-NHa (Figure 4, top). The second one is characterized by a type I β-turn centered on Asp-diamine, with a H-bond between the other malonylCO and diamineNHb (Figure 4, bottom).

As for compound **3**, the ROESY-derived conformation shows a distinct H-bond between NHb and malonylCO, as anticipated on the basis of VT NMR, and an overall type II β-turn conformation on Asp-diamine (Figure 5). Unrestrained MD simulation was performed as reported for **2**.

In addition to the conformation of **3a** shown in Figure 5, the analysis of the trajectories of **3** gave a second conformer, **3b**, whose structure is in agreement with a pseudoinverse γ-turn centered on Asp, and an inverse γ-turn on Arg.[71] This alternative secondary structure (Figure 6) is still compatible with the involvement of the NHb proton in a H-bond as predicted by VT NMR analysis. Despite the different secondary structures, the two conformers, **3a** and **3b**, still maintain a very similar display of the pharmacophores. However, the two situations slightly differ for the distance between the Cβ atoms of Asp and Arg: ~8.3 Å in **3a** and ~8.8 Å in **3b**.

The structures of **2** and **3** share a certain similarity in the RGD-mimetic region. The main difference among the two structures resides in the different orientations of the diamine aromatic side chain and of NHa. In **2**, the aromatic side chain and NHa point above the molecular plane; in **3**, the situation is reversed. In particular, in **2**, the diamine phenyl side chain adopts a pseudoaxial disposition; in **3**, it adopts a pseudoequatorial disposition.

Molecular Docking. To interpret on a molecular basis the different affinities of compounds **2** and **3** for the $\alpha_V\beta_3$ receptor, docking studies were performed using Glide (version 4.5)[72] by starting from the representative macrocycle conformations sampled during the unrestrained MD simulations. Molecular docking of compounds **4**−**9** is discussed in the Supporting Information. The protein binding site was derived from the X-ray crystal structure of the extracellular segment of integrin $\alpha_V\beta_3$ in complex with the cyclic pentapeptide ligand cilengitide [Protein Data Bank (PDB) entry 1L5G].[29] In this X-ray structure, the potent $\alpha_V\beta_3$ antagonist cilengitide, bound to the headgroup of the integrin, features an extended conformation of the RGD

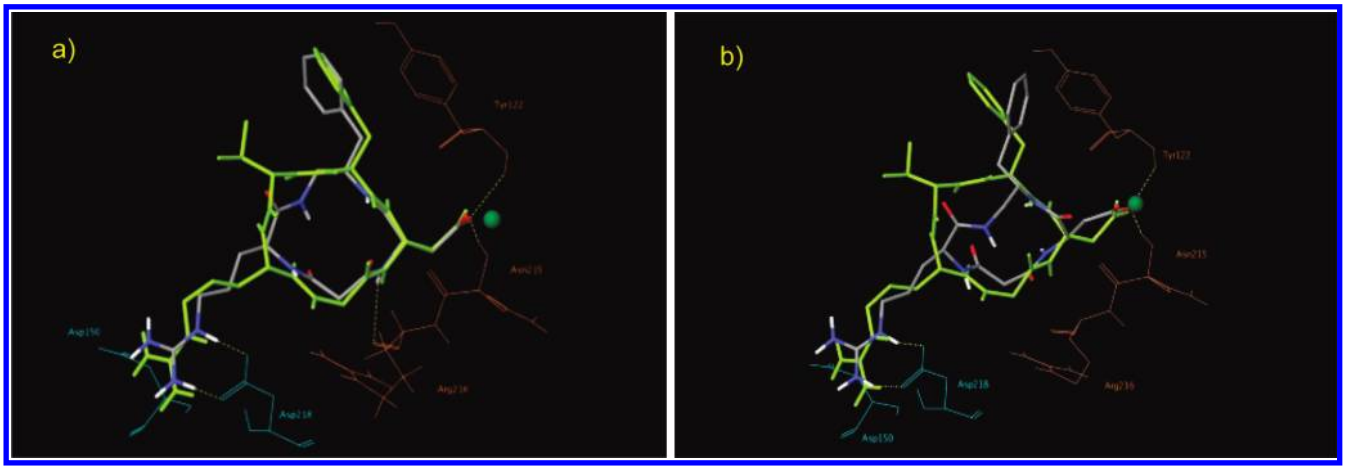

Figure 7. Top-ranked docking poses of (a) ligand **3** (atom color tube representation, macrocycle geometry inverse γ/inverse γ **3b**) and (b) ligand **2** (atom color tube representation, macrocycle geometry β-turn **2b**) into the crystal structure of the extracellular domain of $\alpha_V\beta_3$ integrin (α unit colored cyan and β unit colored orange in a wire representation) overlaid on the bound conformation of cilengitide (green tube representation). Only selected integrin residues involved in the interactions with cilengitide are shown. The Mn^{2+} ion at MIDAS is shown as a green CPK sphere. Nonpolar hydrogen atoms were removed for the sake of clarity.

sequence with a distance of ~9 Å between the C_β atoms of Asp and Arg. The crystal complex interaction pattern involves the formation of an electrostatic clamp between the guanidinium group of the ligand and the negatively charged side chains of Asp^{218} and Asp^{150} in the α unit and between the carboxylic group of cilengitide and the metal cation in the metal ion-dependent adhesion site (MIDAS) region of the β unit. Moreover, further stabilization occurs through hydrogen bonds between the NH group of the ligand Asp residue and the carbonyl oxygen atom of Arg^{216} in the β subunit as well as between the ligand carboxylate oxygen not coordinated to MIDAS and the backbone amides of Asn^{215} and Tyr^{122} in the β unit (Figure 7).

The experimentally observed binding mode of cilengitide with $\alpha_V\beta_3$ integrin was taken as a reference model for the interpretation of the docking results in terms of the ligand-bound conformation and ligand−protein interactions.

The models built for the interaction of compounds **2** and **3** with $\alpha_V\beta_3$ integrin through docking studies showed that suitable macrocycle conformations of these ligands enable them to fit properly in the shallow cleft of the receptor, sharing the binding features of the crystal structure of the cilengitide−$\alpha_V\beta_3$ complex, especially those governing the recognition process. Among the conformations selected from the MD simulations of **2** and **3**, only the macrocycle geometries "inverse γ/inverse γ" **3b** and "β-turn" **2b** generate top-ranked docking poses conserving the relevant ligand−protein interactions observed in the crystal structure of the cilengitide−$\alpha_V\beta_3$ complex. However, the inverse γ/inverse γ geometry of **3b** reproduces the RGD backbone of the X-ray ligand better than the β-turn geometry of **2b** (Figure 7). Moreover, the pseudoequatorial benzyl group in **3b** points to the same direction of the Phe side chain of the reference ligand, that is, toward the outside of the integrin binding site, allowing the aromatic ring to fit unhindered and to form a T-shaped interaction with the Tyr^{122} side chain of the β subunit (Figures 7 and 8).

The β-turn structure of **2b** properly drives the pharmacophoric groups within the binding site to form the key electrostatic interactions with the receptor. Nevertheless, the pseudoaxial benzyl group forces the entire molecule to enter the receptor lopsided. The benzyl group fails in forming

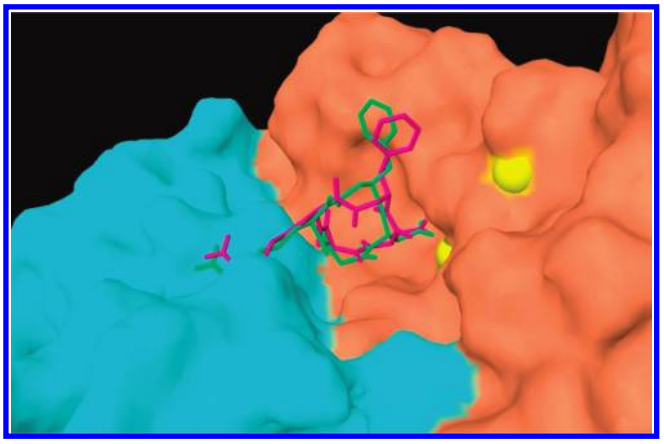

Figure 8. Top-ranked docking poses of mimics **3b** (green tube representation) and **2b** (purple tube representation) in the crystal structure of the extracellular domain of $\alpha_v\beta_3$ integrin represented as a molecular surface (α unit colored cyan, β unit colored orange). Mn^{2+} ions are represented as yellow CPK spheres.

the T-shaped interaction with the aromatic ring of the Tyr^{122} side chain. Accordingly, the Glide score values suggest a slightly better binding for epimer **3**.

Discussion

In this study, a selected minilibrary of stereoisomeric, modified retro-inverso cyclotetrapeptides **2**−**9** having the general structure c[(*S*/*R*)-βPheψ(NHCO)(*S*/*R*)-Aspψ(NHCO)Gly-(*S*/*R*)-Arg] inhibited adhesion of cells to vitronectin- or fibronectin-coated surfaces and inhibited angiogenesis. The different compounds displayed variable activities as $\alpha_v\beta_3$ or $\alpha_5\beta_1$ integrin receptor antagonists, as determined by testing the inhibition of adhesion of fibronectin and vitronectin to $\alpha_v\beta_3$ or $\alpha_5\beta_1$ integrin receptor-expressing cell lines. Interestingly, c[(*S*)-βPheψ(NHCO)Aspψ(NHCO)Gly-Arg] (**2**) displayed a submicromolar activity for $\alpha_5\beta_1$ integrin, and a certain selectivity over $\alpha_v\beta_3$ integrin, while c[(*R*)-βPheψ-(NHCO)Aspψ(NHCO)Gly-Arg] (**3**) was demonstrated to be a potent dual antagonist, with 10^{-8} and 10^{-7} activities for $\alpha_5\beta_1$ and $\alpha_v\beta_3$ integrins, respectively. On the other hand, c[(*S*)-βPheψ(NHCO)(*S*)-Aspψ(NHCO)Gly-(*R*)-Arg] (**4**) and

c[(*R*)-βPheψ(NHCO)(*R*)-Aspψ(NHCO)Gly-(*S*)-Arg] (**8**) revealed moderate micromolar inhibitory activities, while the remaining compounds, **5**−**7** and **9**, were ineffective. These results demonstrate that compound **2** is more specific as an $\alpha_5\beta_1$ integrin antagonist whereas compounds **3**, **4**, and **8** nonselectively antagonized $\alpha_v\beta_3$ and $\alpha_5\beta_1$ integrins, albeit with different efficacies, **3** being the most potent.

Moreover, we showed that $\alpha_5\beta_1$ and $\alpha_v\beta_3$ integrin antagonists inhibited bFGF-induced human endothelial cell tube formation at submicromolar concentrations as examined using the Matrigel assay. Among them, compound **3** showed the most potent antiadhesion and antiangiogenic effects; it can directly interact with $\alpha_v\beta_3$ integrin expressed on melanoma and endothelial cells and can prevent adhesion of endothelial cells to vitronectin displaying higher binding selectivity for $\alpha_v\beta_3$ integrin in cell culture.

Blockade of $\alpha_v\beta_3$ integrin-mediated functions by antibodies or RGD peptides disrupts blood vessel formation in various animal models; $\alpha_v\beta_3$ antagonists may perturb the growth and/or maturation of blood vessels without detectable alteration on the preexisting blood vessels.[73]

Angiogenesis is also directly regulated by binding of fibronectin to its receptor, the $\alpha_5\beta_1$ integrin. Specific antibodies, peptides, and novel nonpeptide antagonists of $\alpha_5\beta_1$ integrin can block angiogenesis induced by several growth factors in both chick embryo and murine models. In fact, these $\alpha_5\beta_1$ antagonists inhibited tumor angiogenesis, thereby causing regression of human tumors in animal models.[74] Antagonists of $\alpha_v\beta_3$ and $\alpha_5\beta_1$ integrins substantially prevent angiogenesis induced by bFGF, suggesting that these integrins regulate similar pathways of angiogenesis.

The results of this study suggest that the partially retro-inverso RGD motif in the cyclotetrapeptide retains the $\alpha_v\beta_3$ and $\alpha_5\beta_1$ integrin antagonist activity. Therefore, we propose that the potent antiangiogenic effect of **3** in cell adhesion and tube formation assays is probably due to the interference of the $\alpha_v\beta_3$ and $\alpha_5\beta_1$ integrin-mediated interactions between endothelial cells and ECM protein. Indeed, **3** significantly decreased the level of bFGF-induced angiogenesis in an in vitro model. Therefore, the mechanism of action of these compounds in suppressing bFGF-elicited angiogenesis could be mediated by the specific blockade of $\alpha_v\beta_3$ ligation. Finally, these integrin antagonists did not cause any cytotoxic effect as evidenced by flow cytometric analysis.

The sequence of peptides **2**−**9** is identical, the only difference being the stereochemistry array. The comparatively higher inhibitory efficacy toward $\alpha_5\beta_1$ integrin observed for compounds **2** and **3**, the most potent of the minilibrary, can be correlated to the specific (*S*,*S*) stereochemistry of the retro-inverso RGD sequence, ψ(NHCO)(*S*)-Asp-ψ(NHCO)-Gly-(*S*)-Arg. Indeed, the remaining compounds possess (*S*,*R*), (*R*,*R*), or (*R*,*S*) (Arg,Asp) configurations.

It is worth mentioning that, due to the partial retro-inverso nature of the RGD sequence, the (*S*,*S*) stereochemistry of Arg and Asp in **2** and **3** leads to overall conformations showing the Arg and Asp pharmacophoric side chains on the opposite sides of the molecular scaffold, an unusual biologically active conformation in comparison to other well-known RGD cyclopentapeptide integrin antagonists, such as c[Arg-Gly-Asp-(*R*)-Phe-Val] or c[Arg-Gly-Asp-(*R*)-Phe-NMeVal] (cilengitide), having the pharmacophoric side chains placed on the same side. Apparently, in the smaller cyclotetrapeptide structures, an opposite orientation allows for a correct distance between the pharmacophores. For both **2** and **3**, during the unrestrained MD simulations, the average distance between Asp and Arg Cβ was ∼8.5 Å, and that between the carboxylate and guanidino functions was ∼13 Å, very similar to that of the $\alpha_5\beta_1$ or $\alpha_v\beta_3$ selective cyclopentapeptides.[29,30,38]

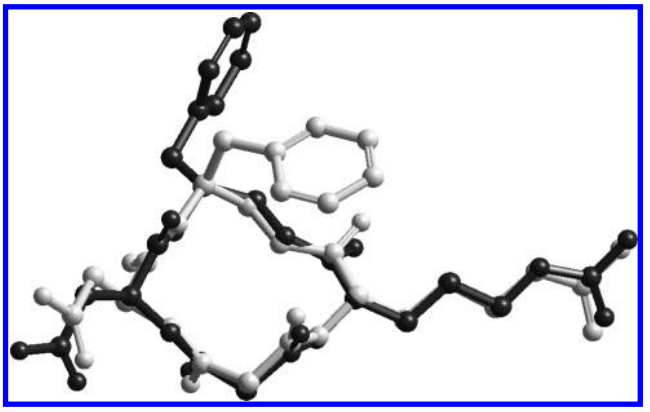

Figure 9. Overlap of the backbone structures of **2** (**2b**, white) and **3** (**3b**, black) determined by ROESY and MD analysis. Side chains have been positioned in the trans extended conformation.

As revealed by conformational analysis (Results), the two compounds show a very similar display of the retro-inverso RGD sequence. On the other hand, the different $\alpha_5\beta_1$ versus $\alpha_v\beta_3$ selectivity displayed by **2** and **3**, sharing the same (*S*,*S*) stereochemistry of the RGD-mimetic sequence, can be attributed to the presence of an (*S*)-diamine in **2** and an (*R*)-diamine in **3**. The most relevant 3D difference can be identified in the disposition of the diamine portion. Apart from the different location of diamine NHa and NHb, in **2** the diamine phenyl side chain adopts an axial position while in **3** it is equatorial (Figure 9).

The experimental 3D structure of $\alpha_5\beta_1$ integrin is not yet available. As a consequence, the comparison of the structures of **2** and **3** with the structures of a few ligands, and with a in silico model, previously reported in the literature, could furnish some useful information about the biologically active conformation at this receptor. Goodman et al. described the receptor-bound conformation of the RGD sequence in the partially ^{15}N-labeled $\alpha_5\beta_1$ integrin weak antagonist c[Mpa^{15}*N*-Arg-^{15}*N*-Gly-^{15}*N*-Asp-^{15}*N*-Asp-^{15}*N*-Val-Cys]-NH_2 (IC_{50} = 1.2 μM), determined by ^{15}N-edited 2D transferred nuclear Overhauser effects.[31] Data were indicative of a tilted conformation, leading to a very short average distance between Arg and Asp Cβ of ∼5.6 Å. More recently, Sewald et al. reported for the $\alpha_5\beta_1$ integrin cyclohexapeptide ligand c[Arg-Gly-Asp-D-Phe-Val-β-Ala] ($IC_{50} = 2 \pm 1$ μM in K562 adhesion assays) a preferred extended RGD conformation showing a quite longer average distance between Arg Cβ and Asp Cβ of ∼9.3 Å.[32] Apparently, the average Cβ−Cβ distance of 8.5 Å observed for **2** and **3** is somewhat between the two values reported above.

More recently, a homology model of the $\alpha_5\beta_1$ integrin has been reported by Kessler, Novellino, and co-workers.[37] The model, obtained by comparative protein modeling and validated with experimental data of nonpeptide ligands, allowed identification of a distance between the carboxylate function and the basic moiety of ∼13 Å. This value is very close to the distance of ∼13.8 Å between the carboxylate and basic groups determined for $\alpha_v\beta_3$ integrin-bound ligands.[20,29,30] As a consequence, the distance between the basic and acid moieties does not constitute a discriminant for $\alpha_v\beta_3$ versus $\alpha_5\beta_1$ selectivity. Therefore, the different pharmacological profile

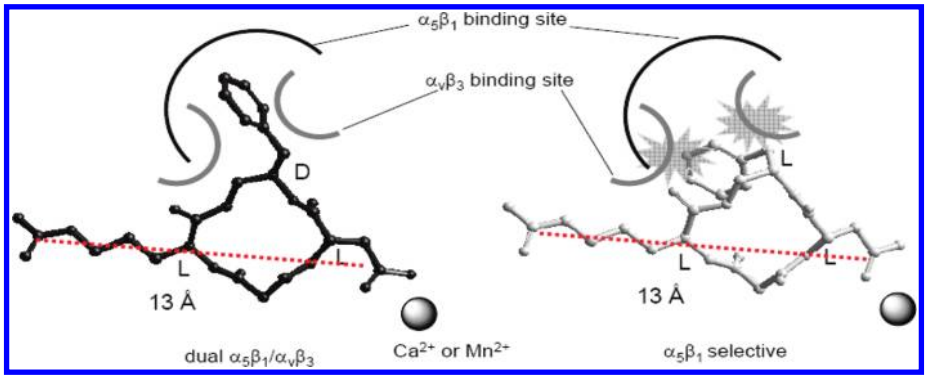

Figure 10. Schematic representation of the proposed disposition of **3** (left, black) and **2** (right, white) within $\alpha_5\beta_1$ (black sticks) and $\alpha_v\beta_3$ (gray sticks) integrin binding site sketches. Unfavorable interactions are also shown (transparent gray flashes).

of **2** and **3** toward $\alpha_v\beta_3$ and $\alpha_5\beta_1$ integrins cannot be explained on the basis of the Cβ−Cβ distance alone.

However, the comparison of $\alpha_5\beta_1$ and $\alpha_v\beta_3$ binding pockets revealed the occurrence of mutated residues in the β subunit. Indeed, (β_3)-Arg^{214} is replaced with (β_1)-Gly^{217}, and (β_3)-Arg^{216} is mutated to (β_1)-Leu^{219}. The substitution of both the bulky Arg residues expands the site of the $\alpha_5\beta_1$ binding pocket in comparison to the $\alpha_v\beta_3$ integrin. The authors concluded that ligands carrying bulky aromatic substituents in the proximity of the Asp (or Asp mimetic) residue can still fit the larger $\alpha_5\beta_1$ binding pocket, but not the cramped $\alpha_v\beta_3$ binding pocket, therefore showing a certain selectivity for $\alpha_5\beta_1$ over $\alpha_v\beta_3$ integrins.

The model highlights the fundamental role of the aromatic residue flanking Asp in determining selectivity. This rationalization is corroborated by the molecular docking computations performed by us on compounds **2** and **3** positioned within the $\alpha_v\beta_3$ integrin receptor binding site (see Results). The results lead to conjecture that the different disposition of diamine side chain is responsible of the different activity of **2** and **3** toward $\alpha_v\beta_3$ integrin.

Molecular modeling studies showed that the pseudoequatorial benzyl group of **3** points toward the outside of the integrin binding site, allowing the aromatic ring to fit unhindered and reproducing the orientation of cilengitide (Results), matching side by side the Tyr^{122} side chain. Conversely, the axial disposition of the benzyl group of **2** gives rise to less favorable interactions, forcing the entire molecule to go into the receptor lopsided.

With regard to the $\alpha_5\beta_1$ integrin, on the basis of the homology model discussed above, the $\alpha_5\beta_1$ integrin seems to be more tolerant in hosting the aromatic side chain of both **2** and **3**. In particular, its larger binding site would more easily accommodate the phenyl ring of **2** with respect to the $\alpha_v\beta_3$ integrin, leading to a pronounced $\alpha_5\beta_1$ selectivity, while the disposition of **3** would be adequate for both integrins, leading to a generally good affinity (Figure 10).

Despite the moderate or absent activity as adhesion inhibitors, compounds **4**−**9** can be utilized to confirm the validity of the model proposed above for the more active compounds, **2** and **3**. Indeed, the structures of **4**−**9** obtained by conformational analysis (see the Supporting Information) in general correlate well with the activity profile of the compounds toward $\alpha_5\beta_1$ and $\alpha_v\beta_3$ integrins. Finally, the different affinities of **4**−**9** for the $\alpha_V\beta_3$ receptor can be explained on the basis of docking analyses performed by Glide (see the Supporting Information).

Conclusions

In summary, we have reported the synthesis of a selected small library of RGD mimetics as $\alpha_v\beta_3$ and/or $\alpha_5\beta_1$ integrin antagonists. The compounds have been designed starting from 13-membered CTP scaffolds based on a partially retro-inverso structure, containing (*S*)- or (*R*)-Asp, (*S*)- or (*R*)-Arg, and an (*S*)- or (*R*)-diamine as a β-Phe surrogate.

The different compounds exhibited variable activities as $\alpha_v\beta_3$ or $\alpha_5\beta_1$ integrin receptor antagonists, as determined by testing the inhibition of adhesion of fibronectin or vitronectin to $\alpha_v\beta_3$ or $\alpha_5\beta_1$ integrin receptor-expressing cell lines. c[(*S*)-βPheψ(NHCO)Aspψ(NHCO)Gly-(*R*)-Arg] (**4**) and c[(*R*)-βPheψ(NHCO)(*R*)-Aspψ(NHCO)Gly-Arg] (**8**) revealed moderate micromolar inhibitory activities; c[(*S*)-βPheψ-(NHCO)Aspψ(NHCO)Gly-Arg] (**2**) displayed a submicromolar activity for $\alpha_5\beta_1$ integrins, and a certain selectivity over $\alpha_v\beta_3$ integrins, while c[(*R*)-βPheψ(NHCO)Aspψ(NHCO)-Gly-Arg] (**3**) was demonstrated to be a potent dual antagonist, with activities of 10^{-8} and 10^{-7} M for $\alpha_5\beta_1$ and $\alpha_v\beta_3$ integrins, respectively, and significantly inhibited bFGF-induced angiogenesis of HUVEC cultured in vitro. The different $\alpha_5\beta_1$ versus $\alpha_v\beta_3$ selectivity of **2** and **3** has been explained on the basis of their alternative secondary structures, discussed on the basis of NMR, ROESY, MD, and molecular docking analyses. In particular, the 3D display of the phenyl substituent of the diamine, pseudoaxial in **2** and pseudoequatorial in **3**, seems to be a major contributor to receptor selectivity.

These $\alpha_v\beta_3$ and $\alpha_5\beta_1$ antagonists may be potentially effective and safe for therapeutic purposes. Small RGD-containing peptidomimetics may be used as lead compounds for developing the potential therapeutic agents for angiogenesis-related diseases, including cancer.

Experimental Section

General Methods. Unless stated otherwise, standard chemicals were obtained from commercial sources and used without further purification. Flash chromatography was performed on silica gel (230−400 mesh), using mixtures of distilled EtOAc and MeOH. Semipreparative RP-HPLC was performed on a C18 column (7 μm particle size, 21.2 mm × 150 mm, from a 7:3 H_2O/CH_3CN mixture to 100% CH_3CN in 15 min) at a flow rate of 12 mL/min. The purity (≥95%) of tested compounds was assessed by analytical RP-HPLC, on an ODS column (4.6 μm particle size, 100 Å pore diameter, 250 mm, DAD 210 nm, from a 9:1 H_2O/CH_3CN mixture to a 2:8 H_2O/CH_3CN mixture in 20 min) at a flow rate of 1.0 mL/min, followed by 10 min at the same composition. ^{1}H NMR spectra were recorded using 5 mm tubes, using 0.01 M peptide at 400 MHz at room temperature.

Solvent suppression was performed by the solvent presaturation procedure implemented in varian (presat). Chemical shifts are reported as δ values relative to the solvent peak. The unambiguous assignment of ^{1}H NMR resonances was performed by gCOSY, HMBC, and HSQC. gCOSY experiments were conducted with a proton spectral width of 3103 Hz. VT ^{1}H NMR experiments were performed over the range of 298−348 K. Peaks were calibrated on DMSO. Conformational rearrangement was excluded since signal broadening was absent. 2D spectra were recorded in the phase sensitive mode and processed using a 90°-shifted, squared sine-bell apodization. ROESY experiments were recorded with a 300 or 350 ms mixing time with a proton spectral width of 3088 Hz.

Representative Synthetic Procedures and Analytical Characterization of PMRI RGD Mimetics 2 and 3. 11. HOBt (0.16 g, 1.2 mmol) was added to a stirred solution of Fmoc-Asp(Mtr)-OH (0.61 g, 1.0 mmol) in a 9:1 DCM/DMF mixture (15 mL) at rt. After 10 min, **10** (0.28 g, 1.0 mmol), EDCI-HCl salt (0.24 g, 1.2 mmol), and TEA (0.40 mL, 3.0 mmol) were added while the mixture was stirred at rt. After 4 h, the mixture was diluted with DCM, and the solution was washed with 0.5 M HCl and saturated Na_2CO_3. The organic layer was dried over Na_2SO_4, and the solvent was removed under reduced pressure. The Fmoc dipeptide **11** was isolated by crystallization from a DCM/Et_2O mixture [0.74 g, 85%, 88% pure by RP-HPLC (see General Methods); R_f = 11.7 min]: ES-MS m/z 875.3 (M + 1), calcd 875.4; ^{1}H NMR (200 MHz, $CDCl_3$) δ 1.40−1.60 (m, 2H), 1.60−1.80 (m, 2H), 2.10 (s, 3H), 2.60 (s, 3H), 2.68 (s, 3H), 2.70−2.78 (m, 3H), 3.00−3.15 (m, 2H), 3.15−3.22 (m, 2H), 3.78 (s, 3H), 4.05 (m, 1H), 4.20 (m, 1H), 4.30−4.50 (m, 2H), 4.99 (s, 2H), 5.45 (br d, 1H), 5.50 (br d, 1H), 5.70 (br s, 1H), 6.10 (br s, 2H), 6.50 (s, 1H), 7.05−7.42 (m, 15H), 7.55 (br d, 2H), 7.75 (br d, 2H).

Fmoc group deprotection was performed by treatment with 2 M DMA in THF (6 mL) at rt. After 30 min, the solution was evaporated at reduced pressure, and the treatment was repeated. After final evaporation of the solution, the residue was triturated twice in *n*-pentane. The deprotected dipeptide [0.50 g, 90%, 86% pure by RP-HPLC (see General Methods); R_f = 8.8 min] was used without further purification: ES-MS m/z 653.3 (M + 1), calcd 653.3.

12. A solution of Meldrum's acid (0.85 g, 6 mmol) and H-Asp(O*t*-Bu)-OBz (1.4 g, 5 mmol) in CH_3CN (15 mL) was warmed to 70 °C under an inert atmosphere. After 3 h, a 4:1 cyclohexane/Et_2O mixture (40 mL) was added, and the oily residue that precipitated was separated. This residue was washed twice with a 4:1 hexane/Et_2O mixture (20 mL), and the resulting dense oil was dissolved in EtOAc (40 mL) and washed with 0.1 M HCl (5 mL). The organic layer was dried over Na_2SO_4, and solvent was evaporated at reduced pressure (<40 °C), giving **12** as a waxy solid, which was used for the following step without further purification (1.2 g, 68%, 84% pure by NMR analysis): ^{1}H NMR (300 MHz, $CDCl_3$) δ 1.31 (s, 9H), 2.72 (dd, J = 5.1, 17.2 Hz, 1H), 2.86 (dd, J = 4.8, 17.2 Hz, 1H), 3.28 (br s, 2H), 4.82 (m, 1H), 5.05 (d, J = 12.1 Hz, 1H), 5.14 (d, J = 12.1 Hz, 1H), 7.25−7.40 (m, 5H), 7.86 (br d, 1H), 9.70−10.4 (br s, 1H).

13. Dipeptides **11** (0.33 g, 0.5 mmol) and **12** (0.18 g, 0.5 mmol) were coupled under the same conditions used for the synthesis of **11** with HOBt (0.082 g, 0.6 mmol), EDCI-HCl salt (0.12 g, 0.6 mmol), and TEA (0.20 mL, 1.5 mmol) in a 9:1 DCM/DMF mixture (10 mL) at rt. After 5 h, the usual workup afforded the fully protected tetrapeptide **13**, isolated by crystallization from a DCM/Et_2O mixture [0.32 g, 65%, 86% pure by RP-HPLC (see General Methods); R_f = 11.2 min]: ES-MS m/z 1001.3 (M + 1), calcd 1001.4; ^{1}H NMR (200 MHz, $CDCl_3$) δ 1.48 (s, 9H) 1.54−1.70 (m, 2H), 1.77 (m, 1H), 1.92 (m, 1H), 2.10 (s, 3H), 2.50 (br s, 1H), 2.70 (s, 3H), 2.76 (s, 3H), 2.74−2.85 (m, 3H), 3.18−3.38 (m, 3H), 3.39−3.50 (m, 3H), 3.90 (s, 3H), 4.10 (m, 1H), 4.60 (m, 1H), 4.93 (m, 1H), 5.03−5.25 (m, 4H), 6.01 (d, J = 8.0 Hz, 1H), 6.20−6.40 (br s, 1H), 6.42 (br s, 2H), 6.60 (s, 1H), 7.18−7.42 (m, 15H), 7.78 (br t, 1H), 7.97 (br d, 1H), 8.10 (br d, 1H); ^{13}C NMR (300 MHz, 9:1 $CDCl_3$/DMSO-d_6) δ 14.5, 17.1, 23.6, 27.3, 29.0, 29.2, 35.5, 37.9, 38.5, 39.8, 48.7, 49.2, 53.3, 55.0, 56.1, 69.6, 73.7, 111.0, 121.3, 125.8, 127.3, 127.3, 127.5, 128.3, 128.3, 128.4, 128.4, 128.6, 128.6, 128.7, 128.7, 130.1, 130.1, 130.6, 132.3, 132.9, 133.8, 136.5, 138.8, 150.2, 157.2, 162.6, 163, 165.7, 167.6, 170.9, 170.9, 172.0, 174.7.

14 {c[*β*Phe*ψ*(NHCO)Asp(O*t*-Bu)*ψ*(NHCO)Gly-Arg(Mtr)]}. Removal of the protecting group from **13** (0.32 g, 0.32 mmol) was performed by treatment with H_2 and catalytic Pd/C in EtOH (15 mL) at rt. After 6 h, the mixture was filtered over Celite, and the solvent was evaporated at reduced pressure, giving the linear tetrapeptide H-*β*Phe*ψ*(NHCO)Asp(O*t*-Bu)*ψ*-(NHCO)Gly-Arg(Mtr)-OH [0.24 g, 96%, 84% pure by RP-HPLC (see General Methods); R_f = 5.9 min], used without further purification: ES-MS m/z 776.3 (M + 1), calcd 776.4.

A mixture of the deprotected tetrapeptide (0.24 g, 0.31 mmol), DPPA (0.15 mL, 0.62 mmol), and $NaHCO_3$ (0.42 g, 5.0 mmol) in DMF (70 mL) was stirred at rt. After 72 h, the solvent was distilled under reduced pressure, the residue was diluted with water, and the mixture was extracted three times with DCM. The solution was evaporated under reduced pressure, and the residue was precipitated from a DCM/Et_2O mixture. Semipreparative RP-HPLC (General Methods) gave **14** [0.16 g, 69%, 96% pure by RP-HPLC (see General Methods); R_f = 8.3 min]: ES-MS m/z 758.5 (M + 1), calcd 758.4; ^{1}H NMR (400 MHz, DMSO-d_6) δ 1.39 (s, 9H, *t*-Bu), 1.40−1.60 (m, 3H, ArgHγ + ArgHβ), 1.70 (m, 1H, ArgHβ), 2.07 (s, 3H, CH_3), 2.29 (dd, J = 10.0, 16.5 Hz, 1H, AspHβ), 2.49 (dd, J = 4.1, 16.5 Hz, 1H, AspHβ), 2.52 (s, 3H, CH_3), 2.62 (s, 3H, CH_3), 2.62−2.85 (m, 2H, diamHβ), 2.95−3.18 (m, 4H, Hc + ArgHδ), 3.18 (d, J = 11.0 Hz, 1H, $COCH_2CO$), 3.26 (d, J = 11.0 Hz, 1H, $COCH_2CO$), 3.81 (s, 3H, OCH_3), 3.85 (m, 1H, diamHα), 4.05 (m, 1H, ArgHα), 4.25 (m, 1H, AspHα), 6.30−6.50 (m, 2H, ArgNHη), 6.46 (d, J = 8.4 Hz, 1H, NHa), 6.70 (s, 1H, 5′-ArH), 6.82 (t, J = 5.4 Hz, 1H, NHb), 6.92 (m, 1H, ArgNHε), 7.15−7.35 (m, 5H, ArH), 8.88 (d, J = 6.6 Hz, 1H, ArgNH), 9.04 (d, J = 6.6 Hz, 1H, AspNH); ^{13}C NMR (400 MHz, DMSO-d_6) δ 18.5, 19.1, 24.0, 25.9, 29.1, 29.3, 36.0, 37.5, 39.1, 39.8, 48.8, 50.4, 51.8, 55.0, 56.3, 73.2, 112.2, 121.3, 125.8, 128.3, 128.3, 128.6, 128.6, 132.6, 132.9, 136.3, 139.2, 162.9, 165.8, 170.9, 170.9, 172.2, 174.7, 175.0.

2 {c[*β*Phe*ψ*(NHCO)Asp*ψ*(NHCO)Gly-Arg]}. The protected cyclotetrapeptide **14** (0.16 g, 0.21 mmol) was treated with a 94:2:1:2:1 mixture of TFA and scavengers [TFA/PhOH/PhSH/H_2O/Et_2S (5 mL)] at rt for 30 min. The mixture was distilled under reduced pressure, and the treatment was repeated. The residue was suspended in Et_2O, and the precipitate was centrifuged. The resulting crude residue was purified by semipreparative RP-HPLC (General Methods), giving **2** [0.077 g, 76%, 97% pure by analytical RP-HPLC (see General Methods); R_f = 1.8 min]: ES-MS m/z 490.2 (M + 1), calcd 490.2; ^{1}H NMR (400 MHz, 8:2 DMSO-d_6/H_2O) δ 1.45−1.60 (m, 3H, ArgHγ + ArgHβ), 1.74 (m, 1H, ArgHβ), 2.30 (dd, J = 9.5, 16.0 Hz, 1H, AspHβ), 2.47 (dd, J = 4.0, 16.0 Hz, 1H, AspHβ), 2.60−2.86 (m, 2H, diamHβ), 2.92−3.20 (m, 4H, Hc + ArgHδ), 3.19 (d, J = 10.8 Hz, 1H, $COCH_2CO$), 3.24 (d, J = 10.8 Hz, 1H, $COCH_2CO$), 3.68 (m, 1H, diamHα), 3.96 (m, 1H, ArgHα), 4.20 (m, 1H, AspHα), 6.70 (d, J = 8.4 Hz, 1H, NHa), 6.90 (br t, 1H, NHb), 7.10−7.35 (m, 5H, ArH), 7.90 (br s, 1H, ArgNHε), 9.10 (br d, 1H, ArgNH), 9.28 (br d, 1H, AspNH); ^{13}C NMR (400 MHz, 8:2 DMSO-d_6/H_2O) δ 26.0, 29.2, 36.5, 37.5, 39.0, 39.8, 40.0, 48.8, 50.2, 51.8, 55.0, 126.0, 128.1, 128.3, 128.8, 128.7, 138.8, 163.9, 171.0, 171.2, 174.7, 175.1, 177.7.

(3) {c[(*R*)-*β*Phe*ψ*(NHCO)Asp*ψ*(NHCO)Gly-Arg]}: ^{1}H NMR (400 MHz, 8:2 DMSO-d_6/H_2O) δ 1.42−1.50 (m, 2H, ArgHγ), 1.56 (m, 1H, ArgHβ), 1.74 (m, 1H, ArgHβ), 2.40 (dd, J = 6.0, 16.8 Hz, 1H, AspHβ), 2.58 (dd, J = 7.2, 16.8 Hz, 1H, AspHβ), 2.75 (dd, J = 6.6, 16.0 Hz, 1H, diamHβ), 2.83 (dd, J = 8.0, 16.0 Hz, 1H, diamHβ), 2.95−3.15 (m, 3H, Hc + ArgHδ), 3.20 (d, J = 10.2 Hz, 1H, $COCH_2CO$), 3.21 (d, J = 10.2 Hz, 1H, $COCH_2CO$),

3.28 (m, 1H, Hc), 3.67 (m, 1H, diamHα), 3.95 (m, 1H, ArgHα), 4.26 (m, 1H, AspHα), 7.02 (br t, 1H, NHb), 7.10−7.35 (m, 5H, ArH), 7.62 (d, $J = 6.9$ Hz, 1H, NHa), 7.90 (br s, 1H, ArgNHε), 8.85 (br d, 1H, ArgNH), 9.22 (br d, 1H, AspNH); ^{13}C NMR (400 MHz, 8:2 DMSO-d_6/H_2O) δ 26.0, 29.0, 34.5, 36.6, 39.3, 39.8, 39.9, 48.8, 50.4, 52.8, 56.6, 124.5, 127.9, 127.9, 129.0, 129.1, 138.8, 163.8, 171.3, 175.0, 175.1, 176.1.

Pharmacological Assays. (i) Materials for Bioassays. Trypsin/EDTA, nonessential amino acids, minimum essential medium (MEM), RPMI-1640 with L-glutamine, antibiotic and antimycotic solution, and glycine were purchased from Invitrogen (Carlsbad, CA). Fetal bovine serum (FBS) and phosphate-buffered saline (PBS) were from Cambrex (Walkersville, MD). Citrate buffer solution, EDTA, DMSO, Triton X-100, 4-nitrophenyl *N*-acetyl-β-D-glucosaminide, phorbol 12-myristate 13-acetate (PMA), pyruvic acid, fibronectin, and vitronectin, both from human plasma, were obtained from Sigma-Aldrich SRL (Milan, Italy). SK-MEL-24 (human malignant melanoma) and K-562 (human erythroleukemia) were obtained from American Tissue Culture Collection (ATCC, Rockville, MD). HUVEC (human umbilical vein endothelial cells) were obtained from Clonetics (Cambrex). Matrigel-precoated 96-well plates and human recombinant bFGF were from BD Biosciences (Bedford, MA).

(ii) Cell Culture. SK-MEL-24 were routinely grown in MEM supplemented with 10% FBS, nonessential amino acids, and sodium pyruvate. K-562 were maintained as a stationary suspension culture in RPMI-1640 and L-glutamine with 10% FBS. HUVEC were cultured in endothelial growth medium (EGM, Clonetics), containing fetal bovine serum, bovine brain extract, human epidermal growth factor, hydrocortisone, gentamicin, and amphotericin B; cells from passages 2−7 were used in this study. Cells were kept at 37 °C in a 5% CO_2 humidified atmosphere. Forty hours before the experiment, K-562 were treated with 25 ng/mL PMA to induce differentiation with an increased level of expression of cell surface antigens.[75]

(iii) Cell Adhesion Assays.[76] Plates (96 wells) (Corning, New York, NY) were coated by passive adsorption with fibronectin (10 μg/mL) or vitronectin (10 μg/mL) overnight at 4 °C. Cells were counted and exposed to different concentrations of each compound for 30 min at room temperature to allow the ligand−receptor equilibrium to be reached. Stock solutions (10^{-2} M) of the assayed compounds were prepared in 33% DMSO in phosphate-buffered saline (v/v); further dilutions were done in PBS alone. The highest concentration of DMSO in the assays was 1% of the stock solution. Control cells were exposed to the same concentration of DMSO. At the end of the incubation time, the cells were plated (50000 cells/well) and incubated at room temperature for 1 h. Then, all the wells were washed with PBS to remove nonadherent cells, and 50 μL of hexosaminidase [4-nitrophenyl *N*-acetyl-β-D-glucosaminide dissolved at a concentration of 7.5 mM in 0.09 M citrate buffer solution (pH 5) and mixed with an equal volume of 0.5% Triton X-100 in water] was added. This product is a chromogenic substrate for β-*N*-acetylglucosaminidase that is transformed in 4-nitrophenol whose absorbance is measured at 405 nm. As previously described,[77] there is a linear correlation between absorbance and enzymatic activity. Therefore, it is possible to identify the number of adherent cells in treated wells, interpolating the absorbance values of the unknowns in a calibration curve. The reaction was blocked by addition of 100 μL of a stopping solution [50 μM glycine and 5 μM EDTA (pH 10.4)], and the plates were read in a Victor^2 Multilabel Counter (Perkin-Elmer, Waltham, MA). Experiments were conducted in quadruplicate and were repeated at least three times. Data analysis and IC_{50} values were calculated using Graph-Pad Prism 3.0 (GraphPad Software, San Diego, CA).

(iv) Flow Cytometry Assay. To assess the amount of intact, apoptotic or necrotic cells, an Annexin V-Fluos (Roche)/propidium iodide (PI) (Sigma-Aldrich) assay was performed. Double staining against annexin V together with PI separates cells, not necrotic, currently undergoing apoptosis from cells that have died of necrosis. HUVEC were treated with different concentrations of the assayed compounds for 30 min at 37 °C; the cells were detached and fixed with 1% paraformaldheyde for 15 min and then washed with PBS. Thereafter, HUVEC were resuspended in Annexin-V-Fluos incubation buffer [10 mM Hepes/NaOH (pH 7.4), 140 mM NaCl, and 5 mM $CaCl_2$] with prediluted Annexin-V-Fluos and PI, according to the manufacturers' instructions. After incubation for 15 min at room temperature in the dark, the cells were analyzed with EPICS XLMCL (Beckman Coulter).

(v) In Vitro Tubular Formation of HUVEC. The endothelial tube formation assay was performed as described.[78] Matrigel-precoated 96-well plates were used, and HUVEC (5000 cells/well) were seeded in the presence of different concentrations of test compounds, in the absence (negative control) or presence of bFGF (30 ng/mL). Cells were incubated for 16 h at 37 °C. After incubation, these cells underwent differentiation into capillary-like tube structures; tube formation was examined by a NIKON microscope equipped with a camera. The experiments were repeated three times.

Conformational Analysis. ROESY intensities were classified very strong, strong, medium, and weak and were associated with distances of 2.3, 2.6, 3.0, and 4.0 Å, respectively. Geminal couplings and other obvious correlations were discarded. For the absence of Hα−COCH_2CO or Hα−NHCH (i, $i + 1$) ROESY cross-peaks, the ω bonds were set at 180° (force constant of 16 kcal mol^{-1} Å^{-2}). Only ROESY-derived constraints were included in the restrained MD. The restrained MD simulations were conducted using the AMBER[70] force field in a 30 Å × 30 Å × 30 Å box of standard TIP3P models of equilibrated water. All water molecules with atoms that come closer to a solute atom than 2.3 Å were eliminated. A 50 ps simulation at 1200 K was used for generating 50 random structures that were subsequently subjected to a 20 ps restrained MD with a 50% scaled force field at the same temperature, followed by 20 ps with full restraints (distance force constant of 7 kcal mol^{-1} Å^{-2}), after which the system was cooled in 5 ps to 50 K. H-Bond interactions were not included, nor were torsion angle restraints. The resulting structures were minimized with 3000 cycles of steepest descent and 3000 cycles of conjugated gradient (convergence of 0.01 kcal Å^{-1} mol^{-1}). The backbones of the structures were clustered by the rmsd analysis module of HyperChem. Unrestrained MD simulation in explicit water was performed for 10 ns at 298 K, at constant temperature and pressure (Berendsen scheme,[79] bath relaxation constant of 0.2).[80] For 1−4 scale factors, van der Waals and electrostatic interactions are scaled in AMBER to half their nominal value. The integration time step was set to 0.1 fs. Box equilibration was set to 10 ps.

Molecular Docking. All calculations were run using the Schrödinger suite of programs (http://www.schrodinger.com) through the Maestro graphical interface.

(i) Protein Setup. The recently determined crystal structure of the extracellular domain of the integrin $\alpha_V\beta_3$ receptor in complex with cilengitide and in the presence of the proadhesive ion Mn^{2+} (PDB entry 1L5G) was used for docking studies. Docking was performed only on the globular head of the integrin because the headgroup of integrin has been identified in the X-ray structure as the ligand-binding region. The protein structure was set up for docking as follows; the protein was truncated to residues 41−342 for chain α and residues 114−347 for chain β. Due to a lack of parameters, the Mn^{2+} ions in the experimental protein structure were modeled via replacement with Ca^{2+} ions. The resulting structure was prepared using the Protein Preparation Wizard of the graphical user interface Maestro and the OPLSAA force field.

(ii) Docking. The automated docking calculations were performed using Glide[72] (Grid-based Ligand Docking with Energetics) within the framework of Impact version 4.5 in a

standard precision mode (SP). The grid generation step started from the extracellular fragment of the X-ray structure of the $\alpha_V\beta_3$ complex with cilengitide, prepared as described in Protein Setup. The center of the grid-enclosing box was defined by the center of the bound ligand. The enclosing box dimensions, which are automatically deduced from the ligand size, fit the entire active site. For the docking step, the size of the bounding box for placing the ligand center was set to 12 Å. No further modifications were applied to the default settings. The Glide-Score function was used to select 20 poses for each ligand. Glide was initially tested for its ability to reproduce the crystallized binding geometry of cilengitide. The program was successful in reproducing the experimentally found binding mode of this compound, as it corresponds to the best-scored pose.

Acknowledgment. We thank MIUR (PRIN 2004) and Bologna University (Funds for Selected Topics) for providing financial support and Stepbio srl, Bologna (Bologna, Italy) for technical support. We also thank Consorzio Spinner for providing a grant to R.D.M. (Project 023/08).

Supporting Information Available: Inhibition of tube formation of HUVEC on Matrigel (Figure S1), $\alpha_v\beta_3/\alpha_5\beta_1$ integrin antagonists that did not induce apoptosis or necrosis in endothelial cells (Figure S2), analytical characterization of PMRI RGD mimetics **4** and **5**, nonobvious ROESY cross-peaks observed for **4** and **5** (Tables S1 and S2), conformational analysis of **4** and **5** in solution, and molecular docking of **4**−**9**. This material is available free of charge via the Internet at http://pubs.acs.org.

References

(1) Brower, V. Tumor angiogenesis, new drugs on the block. *Nat. Biotechnol.* **1999**, *17*, 963–968.
(2) Arndt, T.; Arndt, U.; Reuning, U.; Kessler, H. Integrins in angiogenesis: Implications for tumor therapy. In *Cancer Therapy: Molecular Targets in Tumor-Host Interactions*; Weber, G. F., Ed.; Horizon Bioscience: Norfolk, U.K., 2005.
(3) Curley, G. P.; Blum, H.; Humphries, M. J. Integrin antagonists. *Cell. Mol. Life Sci.* **1999**, *56*, 427–441.
(4) Brooks, P. C.; Clark, R. A.; Cheresh, D. A. Requirement of vascular integrin $\alpha v\beta 3$ for angiogenesis. *Science* **1994**, *264*, 569–571.
(5) Hynes, R. O. A reevaluation of integrins as regulators of angiogenesis. *Nat. Med.* **2002**, *8*, 918–921.
(6) Reynolds, L. E.; Wyder, L.; Lively, J. C.; Taverna, D.; Robinson, S. D.; Huang, X.; Sheppard, D.; Hynes, R. O.; Hodivala-Dikle, K. M. Enhanced pathological angiogenesis in mice lacking $\beta 3$ integrin or $\beta 3$ and $\beta 5$ integrins. *Nat. Med.* **2002**, *8*, 27–34.
(7) Cardarelli, P. M.; Lobl, T. J. Peptide inhibitors of $\beta 1$ integrins. In *Leukocyte Recruitment in Inflammatory Diseases*; Peltz, G., Ed.; Springer: Heidelberg, Germany, 1996; pp 275−294.
(8) Ruoslahti, E. Integrin signaling and matrix assembly. *Tumor Biol.* **1996**, *17*, 117–124.
(9) Okada, N.; Watarai, M.; Ozeri, V.; Hanski, E.; Caparon, M.; Sasakawa, C. A matrix form of fibronectin mediates enhanced binding of *Streptococcus pyogenes* to host tissue. *J. Biol. Chem.* **1997**, *272*, 26978–26984.
(10) Kim, S.; Harris, M.; Varner, J. A. Regulation of integrin $\alpha v\beta 3$-mediated endothelial cell migration and angiogenesis by integrin $\alpha 5\beta 1$ and protein kinase A. *J. Biol. Chem.* **2000**, *275*, 33920–33928.
(11) Ikari, Y.; Yee, K. O.; Schwartz, S. M. Role of $\alpha 5\beta 1$ and $\alpha v\beta 3$ integrins on smooth muscle cell spreading and migration in fibrin gels. *Thromb. Haemostasis* **2000**, *84*, 701–705.
(12) Bewick, M. A.; Lafrenie, R. M. Adhesion dependent signalling in the tumour microenvironment: The future of drug targeting. *Curr. Pharm. Des.* **2006**, *12*, 2833–2848.
(13) Mitjans, F.; Meyer, T.; Fittschen, C.; Goodman, S.; Jonczyk, A.; Marshall, J. F.; Reyes, G.; Piulats, J. Use of gastrin-releasing peptide promoter for specific expression of thymidine kinase gene in small-cell lung carcinoma cell. *Int. J. Cancer* **2000**, *87*, 716–723.
(14) Plow, E. F.; Haas, T. A.; Zhang, L.; Loftus, J.; Smith, J. W. Ligand binding integrins. *J. Biol. Chem.* **2000**, *275*, 21785–21788.
(15) Ruoslahti, E. RGD and other recognition sequences for integrins. *Annu. Rev. Cell Dev. Biol.* **1996**, *12*, 697–715.
(16) Thijssen, V. L. J. L.; van Beijnum, J. R.; Mayo, K. H.; Griffioen, A. W. Identification of novel drug targets for angiostatic cancer therapy; it takes two to tango. *Curr. Pharm. Des.* **2007**, *13*, 3576–3583.
(17) Schmidmaier, R.; Baumann, P. Anti-adhesion evolves to a promising therapeutic concept in oncology. *Curr. Med. Chem.* **2008**, *15*, 978–990.
(18) Ruoslahti, E.; Pierschbacher, M. D. Arg-Gly-Asp: A versatile cell recognition signal. *Cell* **1986**, *44*, 517–518.
(19) DSouza, S. E.; Ginsberg, M. H.; Plow, E. F. Arginyl-glycyl-aspartic acid (RGD): A cell-adhesion motif. *Trends Biochem. Sci.* **1991**, *16*, 246–250.
(20) Henry, C.; Moitessier, N.; Chapleur, Y. Vitronectin receptor $\alpha_V\beta_3$ integrin antagonists: Chemical and structural requirements for activity and selectivity. *Mini-Rev. Med. Chem.* **2002**, *2*, 531–42.
(21) Wermuth, J.; Goodman, S. L.; Jonczyk, A.; Kessler, H. Stereoisomerism and biological activity of the selective and superactive $\alpha_v\beta_3$ integrin inhibitor cyclo(-RGDfV-) and its retro-inverso peptide. *J. Am. Chem. Soc.* **1997**, *119*, 1328–1335.
(22) Cacciari, B.; Spallato, G. Non peptidic $\alpha v\beta 3$ antagonists: Recent developments. *Curr. Med. Chem.* **2005**, *12*, 51–70.
(23) Pfaff, M.; Tangemann, K.; Müller, B.; Gurrath, M.; Müller, G.; Kessler, H.; Timpl, R.; Engel, J. Selective recognition of cyclic RGD peptides of NMR defined conformation by $\alpha IIb\beta 3$, $\alpha V\beta 3$, and $\alpha 5\beta 1$ integrins. *J. Biol. Chem.* **1994**, *269*, 20233–20238.
(24) Gurrath, M.; Müller, G.; Kessler, H.; Aumailley, M.; Timpl, R. Conformation/activity studies of rationally designed anti-adhesive RGD peptides. *Eur. J. Biochem.* **1992**, *210*, 911–921.
(25) Nisato, R. E.; Tille, J.-C.; Jonczyk, A.; Goodman, S. L.; Pepper, M. S. $\alpha_v\beta_3$ and $\alpha_v\beta_5$ integrin antagonists inhibit angiogenesis in vitro. *Angiogenesis* **2003**, *6*, 105–119.
(26) Dechantsreiter, M. A.; Planker, E.; Mathä, B.; Lohof, E.; Hölzemann, G.; Jonczyk, A.; Goodman, S. L.; Kessler, H. N-Metylated Cyclic RGD peptides as highly active and selective $\alpha_v\beta_3$ integrin antagonists. *J. Med. Chem.* **1999**, *42*, 3033–3040.
(27) Cai, W.; Chen, X. Anti-angiogenic cancer therapy based on integrin $\alpha v\beta 3$ antagonism. *Anticancer Agents Med. Chem.* **2006**, *6*, 407–428.
(28) Heckmann, D.; Kessler, H. Design and chemical synthesis of integrin ligands. *Methods Enzymol.* **2007**, *426*, 463–503.
(29) Xiong, J.-P.; Stehle, T.; Zhang, R.; Joachimiak, A.; Frech, M.; Goodman, S. L.; Amin Arnaout, M. Crystal structure of the extracellular segment of integrin $\alpha v\beta 3$ in complex with an Arg-Gly-Asp ligand. *Science* **2002**, *296*, 151–155.
(30) Marinelli, L.; Lavecchia, A.; Gottschalk, K.-E.; Novellino, E.; Kessler, H. Docking studies on $\alpha v\beta 3$ integrin ligands: Pharmacophore refinement and implications for drug design. *J. Med. Chem.* **2003**, *46*, 4393–4404.
(31) Zhang, L.; Mattern, R.-H.; Malaney, T. I.; Pierschbacher, M. D.; Goodman, M. Receptor-bound conformation of the $\alpha 5\beta 1$ integrin antagonist by ^{15}N-edited 2D transferred nuclear Overhauser effects. *J. Am. Chem. Soc.* **2002**, *124*, 2862–2863.
(32) Zimmermann, D.; Guthçhrlein, E. W.; Maleševic′, M.; Sewald, K.; Wobbe, L.; Heggemann, C.; Sewald, N. Integrin $\alpha 5\beta 1$ ligands: Biological evaluation and conformational analysis. *ChemBioChem* **2005**, *6*, 272–276.
(33) Benfatti, F.; Cardillo, G.; Fabbroni, S.; Galzerano, P.; Gentilucci, L.; Juris, R.; Tolomelli, A.; Baiula, M.; Sparta', A.; Spampinato, S. Synthesis and biological evaluation of non-peptide $\alpha_v\beta_3/\alpha_5\beta_1$ integrin dual antagonists containing 5,6-dihydropyridin-2-one scaffolds. *Bioorg. Med. Chem.* **2007**, *15*, 7380–7390.
(34) Takagi, J.; Strokovich, K.; Springer, T. A.; Walz, T. Structure of integrin $\alpha 5\beta 1$ in complex with fibronectin. *EMBO J.* **2003**, *22*, 4607–4615.
(35) Smallheer, J. M.; Weigelt, C. A.; Woerner, F. J.; Wells, J. S.; Daneker, W. F.; Mousa, S. A.; Wexler, R. R.; Jadhav, P. K. Synthesis and biological evaluation of nonpeptide integrin antagonists containing spirocyclic scaffolds. *Bioorg. Med. Chem. Lett.* **2004**, *14*, 383–387.
(36) Kumar, C. C.; Malkowski, M.; Yin, Z.; Tanghetti, E.; Yaremko, B.; Nechuta, T.; Varner, J.; Liu, M.; Smith, E. M.; Neustadt, B.; Presta, M.; Armstrong, L. Inhibition of angiogenesis and tumor growth by SCH221153, a dual $\alpha_v\beta_3$ and $\alpha_v\beta_5$ integrin receptor antagonist. *Cancer Res.* **2001**, *61*, 2232–2238.
(37) Marinelli, L.; Meyer, A.; Heckmann, D.; Lavecchia, A.; Novellino, E.; Kessler, H. Ligand binding analysis for human $\alpha 5\beta 1$ integrin: Strategies for designing new a5b1 integrin antagonists. *J. Med. Chem.* **2005**, *48*, 4204–4207.
(38) Heckmann, D.; Meyer, A.; Marinelli, L.; Zahn, G.; Stragies, R.; Kessler, H. Probing integrin selectivity: Rational design of highly active and selective ligands for the $\alpha 5\beta 1$ and $\alpha v\beta 3$ integrin receptor. *Angew. Chem., Int. Ed.* **2007**, *46*, 3571–3574.

(39) Gentilucci, L.; Cardillo, G.; Tolomelli, A.; Spampinato, S.; Sparta, A.; Squassabia, F. Cyclotetrapeptide mimics based on a 13-membered, partially modified retro-inverso structure. *Eur. J. Org. Chem.* **2008**, 729–735.
(40) Gentilucci, L.; Cardillo, G.; Tolomelli, A.; Squassabia, F.; De Marco, R.; Chiriano, G. Cyclopeptide analogs for generating new molecular and 3D diversity. *Comb. Chem. High Throughput Screening* **2009**, *12*, 929–939.
(41) Schumann, F.; Muller, A.; Koksch, M.; Muller, G.; Sewald, N. Are β-amino acids γ-turn mimetics? Exploring a new design principle for bioactive cyclopeptides. *J. Am. Chem. Soc.* **2000**, *122*, 12009–12010.
(42) Chorev, M.; Goodman, M. A dozen years of retro-inverso peptidomimetics. *Acc. Chem. Res.* **1993**, *26*, 266–273.
(43) Chorev, M. The partial retro−inverso modification: A road traveled together. *Biopolymers* **2005**, *80*, 67–84.
(44) Han, Y.; Giragossian, C.; Mierke, D. F.; Chorev, M. *Ni*-to-*Ni*+3-ethylene-bridged partially modified retro-inverso tetrapeptide β-turn mimetic: Design, synthesis, and structural characterization. *J. Org. Chem.* **2002**, *67*, 5085–5097.
(45) Lee, Y. S.; Agnes, R. S.; Davis, P.; Ma, S.-w.; Badghisi, H.; Lai, J.; Porreca, F.; Hruby, V, J. Partial retro-inverso, retro, and inverso modifications of hydrazide linked bifunctional peptides for opioid and cholecystokinin (CCK) receptors. *J. Med. Chem.* **2007**, *50*, 165–168.
(46) Fletcher, M. D.; Campbell, M. M. Partially modified retro-inverso peptides: Development, synthesis, and conformational behavior. *Chem. Rev.* **1998**, *98*, 763–795.
(47) Glenn, M. P.; Kelso, M. J.; Tyndall, J. D. A.; Fairlie, D. P. Conformationally homogeneous cyclic tetrapeptides: Useful new three-dimensional scaffolds. *J. Am. Chem. Soc.* **2003**, *125*, 640–641.
(48) Norgren, A. S.; Buttner, F.; Prabpai, S.; Kongsaeree, P.; Arvidsson, P. I. β2-Amino acids in the design of conformationally homogeneous *cyclo*-peptide scaffolds. *J. Org. Chem.* **2006**, *71*, 6814–6821.
(49) Maulucci, N.; Chini, M. G.; Di Micco, S.; Izzo, I.; Cafaro, E.; Russo, A.; Gallinari, P.; Paolini, C.; Nardi, M. C.; Casapullo, A.; Riccio, R.; Bifulco, G.; De Riccardis, F. Molecular insights into Azumamide E histone deacetylases inhibitory activity. *J. Am. Chem. Soc.* **2007**, *129*, 3007–3012.
(50) Gentilucci, L.; Cardillo, G.; Tolomelli, A.; De Marco, R.; Garelli, A.; Spampinato, S.; Spartà, A.; Juaristi, E. Synthesis and conformational analysis of cyclotetrapeptide mimetic β-turn templates and validation as 3D scaffolds. *ChemMedChem* **2009**, *4*, 517–523.
(51) Nakabayashi, S.; Warren, C. D.; Jeanloz, R. W. The preparation of a partially protected heptasaccharide-asparagine intermediate for glycopeptide synthesis. *Carbohydr. Res.* **1988**, *174*, 279–289.
(52) Morie, T.; Kato, S.; Harada, H.; Fujiwara, I.; Watanabe, K.; Matsumoto, J.-I. Ring expansion of nitrogen-containing chloromethylheteroalicycles via aziridinium intermediates. *J. Chem. Soc., Perkin Trans. 1* **1994**, 2565–2569.
(53) Conner, S. R.; Scott, G.; Aplin, A. E. Adhesion-dependent activation of the ERK1/2 cascade is by-passed in melanoma cells. *J. Biol. Chem.* **2003**, *278*, 34548–34554.
(54) Park, K.; Kim, Y.-S.; Lee, G. Y.; Parl, R.-W.; Kim, I.-S.; Kim, S. Y.; Byun, Y. Tumor endothelial cell targeted cyclic RGD-modified heparin derivative: Inhibition of angiogenesis and tumor growth. *Pharm. Res.* **2008**, *25*, 2786–2798.
(55) Lundell, B. I.; McCarthy, J. B.; Kovach, N. L.; Verfaillie, C. M. Activation-dependent $\alpha5\beta1$ integrin-mediated adhesion to fibronectin decreases proliferation of chronic myelogenous leukemia progenitors and K562 cells. *Blood* **1996**, *87*, 2450–2458.
(56) Belvisi, L.; Riccioni, T.; Marcellini, M.; Vesci, L.; Chiarucci, I.; Efrati, D.; Potenza, D.; Scolastico, C.; Manzoni, L.; Lombardo, K.; Stasi, M. M.; Orlandi, A.; Ciucci, A.; Nico, B.; Ribatti, D.; Giannini, G.; Presta, M.; Carminati, P.; Pisano, C. Biological and molecular properties of a new $\alpha v\beta3/\alpha v\beta5$ integrin antagonist. *Mol. Cancer Ther.* **2005**, *4*, 1670–1680.
(57) Del Gatto, A.; Zaccaro, L.; Grieco, P.; Novellino, E.; Zannetti, A.; Del Vecchio, S.; Iommelli, F.; Salvatore, M.; Pedone, C.; Saviano, M. Novel and selective $\alpha v\beta3$ receptor peptide antagonist: Design, synthesis, and biological behavior. *J. Med. Chem.* **2006**, *49*, 3416–3420.
(58) Giannis, A.; Rubsam, F. Integrin antagonists and other low molecular weight compounds as inhibitors of angiogenesis: New drugs in cancer therapy. *Angew. Chem., Int. Ed.* **1997**, *36*, 588–590.
(59) Gentilucci, L.; Cardillo, G.; Squassabia, F.; Tolomelli, A.; Spampinato, S.; Sparta, A.; Baiula, M. Inhibition of cancer cell adhesion by heterochiral Pro-containing RGD mimetics. *Bioorg. Med. Chem. Lett.* **2007**, *17*, 2329–2333.
(60) Cheresh, D. A. Human endothelial cells synthesize and express an Arg-Gly-Asp-directed adhesion receptor involved in attachment to fibrinogen and von Willebrand factor. *Proc. Natl. Acad. Sci. U.S. A.* **1987**, *84*, 6471–6475.
(61) Kawaguchi, M.; Hosotani, R.; Ohishi, S.; Fujii, N.; Singh Tulachan, S.; Koizumi, M.; Toyoda, E.; Masui, T.; Nakajima, S.; Tsuji, S.; Ida, J.; Fujimoto, K.; Wada, M.; Doi, R.; Imamura, M. A movel synthetic Arg-Gly-Asp-containing peptide cyclo(-RGDf[dbond]V-) is the potent inhibitor of angiogenesis. *Biochem. Biophys. Res. Commun.* **2001**, *288*, 711–717.
(62) Carmelit, P.; Jain, R. K. Angiogenesis in cancer and other diseases. *Circ. Res.* **2000**, *87*, 176–178.
(63) Liotta, L.; Steeg, P.; Stetler-Stevenson, W. Cancer metastasis and angiogenesis: An imbalance of positive and negative regulation. *Cell* **1991**, *64*, 327–336.
(64) Hanahan, D.; Folkman, J. Patterns and emerging mechanisms of the angiogenic switch during tumorigenesis. *Cell* **1996**, *86*, 353–364.
(65) Kessler, H. Conformation and biological activity of cyclic peptide. *Angew. Chem., Int. Ed.* **1982**, *21*, 512–523.
(66) Stradley, S. J.; Rizo, J.; Bruch, M. D.; Stroup, A. N.; Gierasch, L. M. Cyclic pentapeptides as models for reverse turns: Determination of the equilibrium distribution between type I and type II conformations of Pro-Asn and Pro-Ala β-turns. *Biopolymers* **1990**, *29*, 263–287.
(67) For a leading reference on the use of a cryoprotective DMSO-d_6/H_2O mixture as a biomimetic medium, see: Temussi, P. A.; Picone, D.; Saviano, G.; Amodeo, P.; Motta, A.; Tancredi, T.; Salvadori, S.; Tomatis, R. Conformational analysis of an opioid peptide in solvent media that mimic cytoplasm viscosity. *Biopolymers* **1992**, *32*, 367–372 and references cited herein .
(68) Toniolo, C. Intramolecularly hydrogen-bonded peptide conformations. *CRC Crit. Rev. Biochem.* **1980**, *9*, 1–44.
(69) *HyperChem*, release 8.0.3; Hypercube Inc.: Gainesville, FL, 2007.
(70) Cornell, W. D.; Cieplak, P.; Bayly, C. I.; Gould, I. R.; Merz, K. M.; Ferguson, D. M.; Spellmeyer, D. C.; Fox, T.; Caldwell, J. W.; Kollman, P. A. A second generation force field for the simulation of proteins, nucleic acids, and organic molecules. *J. Am. Chem. Soc.* **1995**, *117*, 5179–5197.
(71) In a preliminary investigation of the conformational features of the PMRI RGD mimetics by ROESY and MD, we analyzed the in-solution structural features of c[βPheψ(NHCO)Asp(O*t*-Bu)ψ-(NHCO)Gly-Arg(Mtr)] (**14**) and c[(*R*)-βPheψ(NHCO)Asp(O*t*-Bu)ψ(NHCO)Gly-Arg(Mtr)], the protected synthetic precursors of **2** and **3**, respectively. While the conformation of fully protected **2** (**14**) was practically coincident to the type I β-turn/ type I β-turn structure of **2** (Figures 5 and 6), the predominant conformation of fully protected **3** was compatible with the inverse γ/inverse γ structure reported in Figure 8. Apparently, increasing the size of the side chains of the PMRI CTPs tends to stabilize the inverse γ/inverse γ structure over the type II β-turn structure (Figure 8).
(72) *Glide*, version 4.5; Schrödinger, LLC: New York, 2007.
(73) Brooks, P. C.; Montgomery, A. M. P.; Rosenfeld, M. Integrin $\alpha_v\beta_3$ antagonists promote tumour regression by inducing apoptosis of angiogenic blood vessels. *Cell* **1994**, *79*, 1157–1164.
(74) Kim, S.; Bell, K.; Mousa, S.; Varner, J. A. Regulation of angiogenesis in vivo by ligation of integrin $\alpha5\beta1$ with the central cell-binding domain of fibronectin. *Am. J. Pathol.* **2000**, *156*, 1345–1362.
(75) Hunakova, L.; Sedlak, J.; Klobusicka, M.; Sulikova, M.; Chorvath, B. Phorbol ester (TPA)-induced differential modulation of cell surface antigens in human pluripotential leukemia (K-562) cell line: Effects of protein kinase inhibitors with broad and PKC selective inhibitory activity. *Neoplasma* **1995**, *42*, 249–253.
(76) Caltabiano, S.; Hum, W. T.; Attwell, G. J.; Gralnick, D. N.; Budman, L. J.; Cannistraci, A. M.; Bex, F. J. The integrin specificity of human recombinant osteopontin. *Biochem. Pharmacol.* **1999**, *58*, 1567–1578.
(77) Shibata, H.; Yagi, T. Rate assay of N-acetyl-β-D-hexosaminidase with 4-nitrophenyl N-acetyl-β-D-glucosaminide as an artificial substrate. *Clin. Chim. Acta* **1996**, *251*, 53–64.
(78) Maeshima, Y.; Manfredi, M.; Reimer, C.; Holthaus, K. A.; Hopfer, H.; Chandamuri, B. R.; Kharbanda, S.; Kalluri, R. Identification of the anti-angiogenic site within vascular basement membrane-derived tumstatin. *J. Biol. Chem.* **2001**, *276*, 15240–15248.
(79) Berendsen, H. J. C.; Postma, J. P. M.; van Gunsteren, W. F.; DiNola, A.; Haak, J. R. Molecular dynamics with coupling to an external bath. *J. Chem. Phys.* **1984**, *81*, 3684–3690.
(80) Jorgensen, W. L.; Chandrasekhar, J.; Madura, J.; Impey, R. W.; Klein, M. L. Comparison of simple potential functions for simulating liquid water. *J. Chem. Phys.* **1983**, *79*, 926–935.